INVESTIGATIONS ON THE PERMEABILITY OF ACRYLIC POWDER STRUCTURES

A THESIS SUBMITTED TO
THE GRADUATE SCHOOL OF NATURAL AND APPLIED SCIENCES
OF
MIDDLE EAST TECHNICAL UNIVERSITY

BY

YASİN AĞIRTOPÇU

IN PARTIAL FULFILLMENT OF THE REQUIREMENTS FOR THE DEGREE OF

MASTER OF SCIENCE

IN

THE DEPARTMENT OF POLYMER SCIENCE AND TECHNOLOGY

SEPTEMBER 2003

Approval of the Graduate School of Natural and Applied Sciences

Prof. Dr. Canan ÖZGEN
Director

I certify that this thesis satisfies all the requirements as a thesis for the degree of Master of Sciences.

Prof. Dr. Ali USANMAZ
Head of Department

This is to certify that we have read this thesis and that in our opinion it's fully adequate, in scope and quality, as a thesis for the degree of Master of Science in Polymer Science and Technology.

Prof. Dr. Erdal BAYRAMLI
(Supervisor)

Examining Committee in Charge

Prof. Dr. Leyla ARAS (Chairman) _____

Prof. Dr. Erdal BAYRAMLI _____

Prof. Dr. Vasıf HASIRCI _____

Prof. Dr. Önder ÖZBELGE _____

Assist. Prof. Dr. Göknur BAYRAM _____

ABSTRACT

INVESTIGATIONS ON THE PERMEABILITY
OF
ACRYLIC POWDER STRUCTURES

AĞIRTOPÇU, Yasin
M.S., Department of Polymer Science and Technology
Supervisor : Prof. Dr. Erdal BAYRAMLI

September 2003, 71 pages

There are many examples where creation and usage of porous substrates play important roles in various fields of application in material science and technology. In the manufacture of ceramic products, as an alternative to the plaster molds, porous resin molds are used in order to resolve the drawbacks that result from plaster mold cementation.

A porous substrate can be produced by various ways. In this study, porous polymeric matrices of poly(methyl methacrylate) (PMMA) and poly(methyl methacrylate-co-2-hydroxyethyl methacrylate) [poly(MMA-HEMA)] polymers were prepared by connecting the polymer microspheres to each other by an epoxy adhesive. To improve the surface properties, methyl methacrylate (MMA) was copolymerized with 2-hydroxyethyl methacrylate (HEMA). The microspheres used were synthesized by suspension polymerization and characterization was

done by Nuclear Magnetic Resonance (NMR), Particle Size Analyzer and Scanning Electron Microscope (SEM). The porous samples were prepared with PMMA and poly(MMA-HEMA) copolymer microspheres with two different HEMA contents and their surface energies were measured. In addition, the effect of mean particle diameter of the microspheres used and the epoxy content of the solution used to bind the microspheres, on the impregnation capacity, morphology and the impact strength of the porous samples prepared, were studied.

Inclusion of HEMA into the formulation improved the impregnation capacity of the samples. Using microspheres with narrower particle size distribution resulted in larger representative capillary radii and higher rate of impregnation of the samples. Increasing the epoxy content of the solution used to bind the beads, increased the impact strengths of the samples prepared.

Keywords : sphere packing, porous polymeric matrices, surface energy, capillary impregnation.

ÖZ

AKRİLİK TOZLARDAN OLUŞAN YAPILARIN
GEÇİRGENLİK ÖZELLİKLERİ ÜZERİNE ÇALIŞMALAR

AĞIRTOPÇU, Yasin
Y.L., Polimer Bilimi ve Teknolojisi Bölümü
Tez Yöneticisi : Prof. Dr. Erdal BAYRAMLI

Eylül 2003, 71 sayfa

Gözenekli substratların eldesi ve kullanımının malzeme bilimi ve teknolojisinin çeşitli uygulama alanlarında önemli rol oynadığı birçok örnek vardır. Seramik ürünlerinin üretiminde, alçı kalıp kullanımından doğan olumsuzlukları çözmek amacıyla alçı kalıplara alternatif olarak gözenekli reçine kalıplar kullanılmaktadır.

Gözenekli bir substrat çeşitli yollarla üretilebilir. Bu çalışmada, poli(metil metakrilat) (PMMA) ve poli(metil metakrilat-2-hidroksietil metakrilat) [poli(MMA-HEMA)] polimerlerinin gözenekli polimer matrisleri polimer mikroküreciklerinin bir epoksi yapıştırıcı ile birbirlerine bağlanması ile hazırlanmıştır. Yüzey özelliklerini geliştirmek için metil metakrilat (MMA), 2-hidroksietil metakrilat (HEMA) ile kopolimerleştirilmiştir. Kullanılan mikroküreciklер süspansiyon polimerleşmesi ile sentezlenmiş ve Nükleer Manyetik Rezonans (NMR), Tanecik Boyutu Analizi ve Tarayıcı Elektron

Mikroskobu (SEM) ile karakterizasyonu yapılmıştır. Gözenekli polimer numuneleri PMMA ve iki farklı HEMA içerikli poli(MMA-HEMA) kopolimerlerinin mikroküreciklerı ile hazırlanmış ve bunların yüzey enerjileri ölçülmüştür. Ayrıca, kullanılan mikroküreciklerin ortalama tanecik boyutunun ve mikroküreciklerı yapıştırmakta kullanılan çözeltinin epoksi içeriğinin hazırlanan gözenekli numunelerin emme kapasitesi, yüzey özellikleri ve darbe dayanımı üzerindeki etkileri çalışılmıştır.

Formülasyon içine HEMA dahil edilmesi numunelerin emme kapasitesini geliştirmiştir. Tanecik boyutu dağılımı daha dar olan mikroküreciklerin kullanımı, hazırlanan numunelerin eşdeğer kapiler yarıçapının daha geniş ve emme hızının daha yüksek olması ile sonuçlanmıştır. Mikroküreciklerı birleştirmek için kullanılan çözeltinin epoksi içeriğinin artırılması hazırlanan örneklerin darbe dayanımını artırmıştır.

Anahtar Kelimeler : küre paketleme, gözenekli polimer matrisleri, yüzey enerjisi, kapiler emme.

To my family

ACKNOWLEDGEMENTS

I would like to express my deepest gratitude to my supervisor Prof. Dr. Erdal BAYRAMLI for his guidance, patience, advice, encouragement and endless support throughout this study.

I would like to thank with all my heart to my love and fiancée Dilek Selvet for her love, and moral support during my studies.

I wish to express my sincere thanks to Tuncay Baydemir for his friendship, help and valuable discussion.

I am also thankful to Elif Vargün, Selahattin Erdoğan, Zeynep Duru, Güralp Özkoç, Aysel Kızıltay, and all my friends for their helps and support.

Finally, I would like to express my sincere thanks to my family for their great sacrifice, unshakeable faith and moral support during my education.

TABLE OF CONTENTS

LIST OF TABLES

TABLE

LIST OF FIGURES

FIGURE

CHAPTER 1

INTRODUCTION

The creation of porous substrates is of great interests in various fields of application in material science and technology. The production of pores of different sizes is carried out by various means. One way to achieve this aim is the use of porogens which are usually low boiling liquids. In the polymerization process the volatile liquid creates a porous structure as solidification progresses. Another method is selective solubilization of the solid by means of an etching type liquid as in the case of glass substrates or polymers with amorphous and crystalline components [1].

Although effective, these two methods do not provide the controlled level of porosity, the end result is unpredictable in terms of pore size, amount or shape. A third way of creating porous substrates is through the packing of spherical particles. As it is well-known the pore space amongst identical spheres in close-packed structures is 26%. In the case of random packing of identical or multimodal polydisperse spheres the porosities achieved are from 50% to 65% as determined from experimental studies [2].

The required rigidity to porous substrates composed of spherical particles is achieved by the use of an adhesive that binds the spheres to each other through the touch points as explained in Section 1.4.

In the sphere packing method there is no limitation on the size and the thickness of the substrate produced and it is possible to adjust the pore percentage and pore size by a judicious choice of sphere diameters and the polydispersity of the sphere sizes. The spheres can be prepared from nano sizes to the fraction of millimeter size by different methods. In this study suspension polymerized poly(methyl methacrylate) (PMMA) and poly(methyl methacrylate-co-2-hydroxyethyl methacrylate) [Poly(MMA-HEMA)] spheres were used. The sphere size can be adjusted by varying the stirring rate, viscosity ratio and the interfacial tension between the aqueous phase and the monomer phase and the temperature of polymerization.

The pressure difference, ΔP, created in capillary impregnation is given by Laplace equation [3]; if gravity is neglected,

$$\Delta P = \gamma \cos\theta \, (1/R_1 + 1/R_2) \qquad (1)$$

where R_1, R_2 are the principal radii of curvature, γ, the interfacial tension and θ is the contact angle at the interface. For axisymmetric interfaces $R_1 = R_2$ and hence

$$\Delta P = 2 \gamma \cos\theta / R \qquad (2)$$

The Laplace equation shows that the pressure created is inversely proportional to capillary radius and linearly proportional to γ and $\cos\theta$. These are the parameters to be studied to optimize impregnation rates in any study. The contact angle has to be smaller than 90^0 to have any impregnation at all and smaller the capillary radius the larger the capillary pressure that is responsible for impregnation.

One interesting application of PMMA porous matrices is their use as mold material in ceramic production instead of calcium sulphate which increases the rate of production of whiteware 3 to 4 fold because of high impregnation rates and ease of re-use.

When ceramic forming techniques are considered in terms of industry, it is seen that there are some techniques like pressing or casting into a plaster mold that are based on mass production. The reason for the usage of plaster is the plaster's ability to absorb the water in the mud and to make the mud stick on the surface and dry to form a wall-thickness. However, using ceramic plaster mold has some drawbacks, such as low production rate, short life of the mold, low quality of the produced article, etc. To resolve these drawbacks resulted from ceramic plaster mold cementation, another technique, high-pressure cementation is used recently. Different from conventional plaster shaping, high-pressure cementation replaces the plaster mold by using a porous resin mold. Because the high-strength resin mold is porous, during cementation the water content within the slurry can be force-driven from the holes of the mold by means of pressure. Consequently, the cementation speed is faster, the texture of the body is finer and more uniform, and the quality is more enhanced substantially than the plaster shaping [4].

1.1. Methacrylic Polymers

The nature of the R group in methacrylic acid ester monomers having the generic formula $CH_2=C(CH_3)COOR$ generally determines the properties of the corresponding polymers. Methacrylates differ from acrylates in that the α-hydrogen of the acrylate is replaced by a methyl group. This methyl group imparts stability, hardness and stiffness to methacrylic polymers. The methacrylate monomers are extremely versatile building blocks. They are moderate-to-high boiling liquids that readily polymerize or copolymerize with a variety of other

monomers. All of the methacrylates copolymerize with each other and with the acrylate monomers to form polymers having a wide range of hardness; thus polymers that are designed to fit specific application requirements can be tailored readily. The properties of the copolymers can be varied to form extremely tacky adhesives, rubbers, tough plastics, and hard powders. Although higher in cost than many other common monomers, the methacrylates' unique stability characteristics, ease of use, efficiency, and the associated high quality products often compensate for their expense [5].

Methacrylate polymers have a greater resistance to both acidic and alkaline hydrolysis than do acrylate polymers; both are far more stable than poly(vinyl acetate) and vinyl acetate copolymers. There is a marked difference in the chemical reactivity among the noncrystallizable and crystallizable forms of poly(methyl methacrylate) relative to alkaline and acidic hydrolysis. Conventional (ie, free-radical), bulk-polymerized, and syndiotactic polymers hydrolyze relatively slow compared with the isotactic type [6]. Polymer configuration is unchanged by hydrolysis. Complete hydrolysis of nearly pure syndiotactic poly(methyl methacrylate) in sulfuric acid and reesterification with diazomethane yields a polymer with an nmr spectrum identical to that of the original polymers. There is a high proportion of syndiotactic configuration present in conventional poly(methyl methacrylate) which contributes to its high degree of chemical inertness [5].

1.1.1. Poly(methyl methacrylate) (PMMA)

Otto Rohm and Otto Haas pioneered the commercial application of acrylate and methacrylate polymers. Their first commercial (meth)acrylate product was a polyacrylic interlayer for safety glass in 1928. This was shortly followed by cast PMMA sheet initially used in both North America and Europe for aircraft glazing

during the Second World War. The sheets were cast between two glass plates and then heated and vacuum-formed to the shape of aircraft canopies. Shortly after the war, new markets for PMMA sheets in glazing and lighting fixtures arose. At about that time molding pellets were introduced into many automotive applications, once heat and light stable colorants were found. In the 1960s processes for continuous casting of sheet and continuous bulk polymerization to yield pellets were commercialized. During the early 1980s continuous melt-calendered sheet was developed and replaced cell cast sheet in many applications where lower cost was a factor.

The structure of PMMA is:

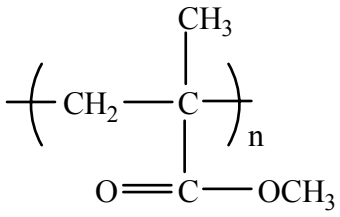

PMMA is made commercially by four different polymerization methods: bulk casting, suspension polymerization, bulk polymerization, and emulsion polymerization. Each of these methods utilizes free radical chemistry. Other forms of polymerization (for example, anionic, group transfer, and other types of ‘‘living’’ polymerizations) are known but are not commercially important today.

In the suspension polymerization process, beads of monomer are formed in de-ionized water by continuous agitation. The size of the bead is determined by the rate of agitation, the presence of dispersants, and other components. Peroxy or azo initiators are used. Polymerization temperatures are usually kept below 100 ^{0}C. During polymerization the polymer is formed and remains dissolved in the monomer droplets. The partially converted droplets become sticky between about 20% and about 80% conversion requiring the presence of dispersing agents to

stabilize the suspension and prevent agglomeration of the beads. The reactions are driven to high conversion. The resulting beads of polymer can be used as is.

The glass transition temperature of PMMA depends on the chain tacticity and can range from about 45 ^{0}C for isotactic PMMA to greater than 130 ^{0}C for syndiotactic PMMA. Tacticity of PMMA depends on the method and temperature of polymerization. Tacticity of anionically polymerized PMMA is strongly influenced by the solvent and cationic species used and can be adjusted over a wide range. The tacticity of emulsion-made PMMA is usually 50-70% syndiotactic, ~30% atactic and ~10% or less isotactic. Commercial bulk polymerized PMMA has a T_g in the 110-115 ^{0}C range.

Polymers made from PMMA and copolymers that are largely PMMA are used primarily in plastic applications. These PMMA products have a unique combination of properties including crystal clarity, resistance to light and weathering, breakage resistance, and mechanical strength, making them unique among plastics. The hardness of PMMA allows it to be substituted for glass, metals, and wood in many applications [7].

1.1.2. Poly(2-hydroxyethyl methacrylate) (PHEMA)

Hydrophilic gels are a very important class of polymeric materials with extensive applications as biomedical products. The first prepared and described polymer hydrogels for biomedical application were proposed by Wichterle and Lim. They used 2-hydroxyethyl methacrylate (HEMA) as the monomer in their development. The most widely used hydrogel in hydroxyalkyl methacrylates or acrylates is PHEMA.

The structure of PHEMA is :

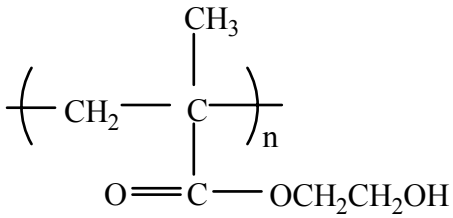

To form a gel that is hydrophilic but insoluble in water, the HEMA must be copolymerized with a crosslinking agent in aqueous solution. PHEMA is usually prepared by free radical solution polymerization. Simultaneous copolymerization and crosslinking reaction in solution is the prefered method to prepare PHEMA since the polymerization rate is fast and the shape of gels can be controlled. The free radicals for the polymerization of HEMA are generated by chemical initiators, ionizing radiation, or photochemical initiators [8].

1.2. Surface Free Energy

The surface free energy of solids is an important parameter for understanding, interpreting, and predicting surface phenomena such as adsorption, wetting, and adhesion. Surface energies are responsible for the behavior and properties of common materials such as paints, adhesives, detergents, and lubricants. Surface free energy analyses have been extensively used by researchers in many diverse studies of solids such as polymers with respect to, for example, their relation to surface composition, characterization of hydrophilic-hydrophobic polymeric surfaces, the stability of polymer surfaces subjected to UV irradiation, etc.

In view of the poor mobility of molecules in a solid, its surface energy cannot be determined directly. Indirect methods of determination based on

wettability phenomena have been developed for this purpose. Thus the method based on contact angle measurements in appropriately chosen test liquids provides a simple and convenient technique for examining the immediate surface of low-energy solids such as polymers. It has been used to determine the components of the surface free energies of solids and to study adhesion of liquids to solid surfaces. The contact angle depends on many factors including vapor pressure of the liquid, properties of liquid films on the solid, and the method of measurement. The interpretation of contact angle, even for clean liquids, is not always easy and at times even impossible without the introduction of many assumptions and approximations. In many cases interpretation of contact angles is made easier when surface free energy is considered to be consequence of dispersive, dipole-dipole, dipole-induced dipole, hydrogen bonding, π-bonding, electrostatic, and donor-acceptor interactions. For practical reasons, it is common to include all the nondispersive interactions in a single term. Thus the surface free energy could be divided into dispersive and nondispersive components in its calculation [9].

Contact angle measurements have been made for determining the wettability of various materials. This angle is characteristic of the substances in the system due to surface tension of the liquid and the surface energy of the solid. Low contact angle indicates good wettability. As the contact angle increases, the wettability decreases.

Experimental measurement of the contact angles enables the parameters such as polar (acid-base) and non-polar (dispersive) components to be calculated. The liquid thus acts as a sensitive probe by interacting chemically with functional groups at the surface [10].

The total surface free energy (γ_S^{TOT}) of a given solid material (s) can be considered as composed of two parts: the Lifshitz-van der Waals (γ_S^{LW}) and the Lewis acid-base (γ_S^{AB}) components [11]. The former represents the dispersion

forces, dipole-dipole (Keesom) and induction (Debye), and the latter represents the short range H-bonding or acid-base interaction. This is written as the sum of the two components:

$$\gamma_S^{TOT} = (\gamma_S^{LW}) + (\gamma_S^{AB}) \qquad (3)$$

where the acid-base term is a property that depends on the material interaction of two unlike species, an acid and a base. (γ_S^{AB}) is composed of two surface parameters, which are independent of the physical presence of one another : (γ_S^{+}), the Lewis acid component, and (γ_S^{-}), the Lewis base component of the surface free energy. These, together, yield the acid-base component of the surface free energy (γ_S^{AB}):

$$(\gamma_S^{AB}) = 2\,(\gamma_s^{+}\ \gamma_s^{-})^{1/2} \qquad (4)$$

The most characteristic feature of these Lewis acid and base components is that they are not additive although the non-polar ones are. (it means that if a phase(s) possesses only (γ_s^{+}) or (γ_s^{-}), this component does not participate in the total surface free energy of the phase(s)). However, this component interacts with the complementary components of other phases. As a result, the total surface free energy of a phase(s) is:

$$\gamma_S^{TOT} = (\gamma_S^{LW}) + (\gamma_S^{AB}) = \gamma_S^{LW} + 2\,(\gamma_s^{+}\ \gamma_s^{-})^{1/2} \qquad (5)$$

The values of γ_S^{AB}, γ_s^{+}, γ_s^{-} can be determined by using the contact angle (θ) subtended by a liquid on a solid surface and the 'Complete Young Equation' [12]:

$$(1+\cos\theta)\ \gamma_L^{TOT} = 2[(\gamma_L^{LW}\gamma_S^{LW})^{1/2} + (\gamma_L^{-}\ \gamma_S^{+})^{1/2} + (\gamma_L^{+}\ \gamma_S^{-})^{1/2}] \qquad (6)$$

where θ is the contact angle of the test liquid and γ_L^{TOT} is the surface tension of the test liquid. The Lifshitz-van der Waals (LW) component of a solid surface can be found from the contact angle of a non-polar liquid (θ_{NP}), where $\gamma_l^{TOT} = \gamma_l^{LW}$ on the solid surface. In this case, the equation reduces to:

$$(1+\cos\theta_{NP})\ \gamma_L^{TOT} = 2[\gamma_L^{LW}\gamma_S^{LW}]^{1/2} \qquad (7)$$

As a result, the LW component of a solid surface can be calculated by applying the contact angle of a non-polar liquid on the surface of this solid by using the Equation (7).

For a bipolar liquid with surface tension γ_1, acidic and basic surface parameters γ_1^+ and γ_1^- respectively, and non-polar surface component γ_1^{LW}, the equation corresponding to Equation (7) is:

$$(1+\cos\theta_1)\ \gamma_1^{TOT} = 2[(\gamma_1^{LW}\gamma_S^{LW})^{1/2} + (\gamma_1^+\ \gamma_S^-)^{1/2} + (\gamma_1^-\ \gamma_S^+)^{1/2}] \qquad (8)$$

and for a second bipolar liquid with surface parameters γ_2^+, γ_2^- and γ_2^{LW}, the equation corresponding to Equation (7) is:

$$(1+\cos\theta_2)\ \gamma_2^{TOT} = 2[(\gamma_2^{LW}\gamma_S^{LW})^{1/2} + (\gamma_2^+\ \gamma_S^-)^{1/2} + (\gamma_2^-\ \gamma_S^+)^{1/2}] \qquad (9)$$

Equations (8) and (9) constitute a set of two simultaneous equations in terms of the parameters of the solid γ_S^+, γ_S^- and γ_S^{LW} and the two contact angles θ_1 and θ_2 that are measured on the solid surface. These equations are then solved for γ_S^+, γ_S^- with the known γ_S^{LW}, provided the γ_1^+, γ_1^-, γ_1^{LW}, γ_2^+, γ_2^- and γ_2^{LW} for the probe liquids are known [10].

1.3. Random Packing of Spheres

Random packings of spheres with constant and random diameters play an important role in many branches of physics and engineering. Simulated packings serve as models for real packings of particles, e.g. in the context of particle science, where, however, the assumption that the particles are spheres is often a simplification. Also many porous media can be represented as packed arrangements of spheres [13].

Packing problems of solid particles are frequently encountered in a wide field of science and technology. Both the packing porosity and the number of contacts between neighbor particles have an essential relation to the material and the process properties of solid particles. Many experimental studies have been done of the fractional void volume of a bed of solid particles, and it is a well-known empirical fact that the packing porosity varies with the size distribution of the materials involved. From a theoretical point of view, on the other hand, much work has been devoted to the regular packings of solid spheres, and a few investigators have examined the mixture porosity of a bed of solid particles of different sizes. Until now, however, nobody has succeeded in generally describing the mixture porosity as a function of the size distribution of particles [14].

One of the most important physical properties of a multiparticle solid system is the packing density. This is defined as the volume fraction of the system which is occupied by solids, and is equal to 1.0 minus the porosity of the system. Where the density of the interparticle fluid is negligible the packing density is the ratio of the bulk density of the system to the true density of the solid particles.

It has been repeatedly shown that the packing density of a fixed bed is a function of the particle size distribution, particle shape, the mode of packing, the size of the system boundary, and, indirectly, the absolute size of the particles.

Tickell et al. using systems of unconsolidated sand failed to obtain a satisfactory correlation between bed porosity and the skewness of the size distribution. Fancher et al. report some porosity values for sands of different distributions, but because of wide diversity of shape between different samples no direct correlation of porosity with size distribution was possible. Cloud , following a study of particle size distribution and porosity of various oil and stones, concluded that there was a qualitative relation between porosity and the coefficient of uniformity of the particle size.

Bo et al. report some porosity values for synthesized size distributions. Their results indicate that for powders of the same size limits, the porosity of a packed bed decreases as the cumulative size distribution approaches linearity when plotted on ordinary decimal coordinates, and that powders with a wider size range have a lower porosity than those with similar form of distribution but having narrower size limits [15].

It appears that as particle size decreases, friction, adhesion and other surface forces become increasingly important since the surface area to volume ratio of the material increases markedly. These factors could be expected to contribute to bridging and arching in the particle system and, consequently, to produce increasing levels of porosity with decreasing particle size.

In practice, in nature or in industry, particulate material is usually of several sizes. It may be possible to select quantities and sizes in such a way as to produce an optimum packing of particles of given size distribution is required. The special case is based on the simple concept that the interstices in a packing of particles of a given size may be occupied by smaller particles, thus diminishing the overall voidage [16].

1.4. Liquid Bridge Formation Between Spheres

Two spheres can be connected to each other by the formation of a liquid bridge at the contact point as shown in the following figure.

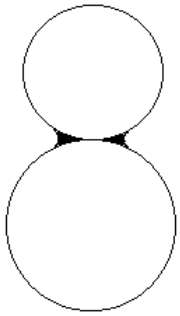

Figure 1.1. Connection of two spheres by the formation of an epoxy bridge at the contact points.

The amount of force that results from such a configuration was studied by Bayramlı and van de Ven [17]. If the liquid bridge contains an adhesive, as the solvent evaporates a permanent attachment forms between the two spheres. When this process is carried out in a randomly packed sphere bed, a three dimensional inter-connected network of spheres are formed. This is the approach used in the present study to create porous substrates.

1.5. Spontaneous Penetration of Liquids into Capillaries

When a capillary or a porous body is set in contact with a wetting fluid, the fluid spontaneously wets the pore walls and penetrates inside. This phenomenon is observed in many natural and physiological processes and has numerous technological applications in oil and gas recovery, civil engineering, agriculture, catalysis, paper and fiber industries, and so forth. Despite its apparent simplicity

and more than 80-year history of intense studies, the problem of spontaneous penetration still attracts considerable attention and opens new challenges for physicists, chemists, and engineers.

Spontaneous liquid imbibition is caused by the forces of attraction between fluid and solid. It occurs when the free energy of the solid–gas interface exceeds the free energy of the solid–liquid interface. Therefore, wetting leads to a reduction of the total free energy of the system. An interplay of intermolecular interactions in the vicinity of the three-phase contact line gives rise to a macroscopic wetting force which depends on the surface tension of the liquid, γ, the pore radius, r , and the contact angle, θ. The latter is an effective parameter characterizing a given solid–liquid–gas system. For wetting fluids, $\theta < 90^0$. In cylindrical capillaries, the wetting force, expressed as the pressure difference across the liquid–gas interface, is given by the Laplace equation, $P_L = 2 \gamma \cos\theta / r$. The imbibition ceases when the wetting force is balanced by an external force—in particular, gravity. The equilibrium height of the liquid rise in a capillary is given by $l_{cap} = 2 \gamma \cos\theta / \rho g r$, with ρ being the fluid density and g the gravity.

Since the work of Lucas and Washburn, the dynamics of imbibition has been described by balancing the wetting force by the gravity and the viscous Poisseuillian resistance. In so doing, the motion of the liquid column in a vertical cylindrical capillary is governed by the Lucas–Washburn (LW) equation:

$$(8\eta / \rho r^2)x \, dx / dt = 2 \gamma \cos\theta / \rho r - gx \qquad (10)$$

Here, the column height is denoted by x and the fluid viscosity by η. The LW equation of the imbibition dynamics in porous solids has the same structure with effective parameters of permeability and hydraulic radius.

The LW equation has proved adequate for the uptake of viscous fluids in capillaries and porous solids of a relatively large extension in the direction of flow. Whenever the gravity factor is insignificant so that the inequality $x \ll 2\gamma\cos\theta / (\rho g r)$ holds, the scaling relation between the depth of penetration and time takes the form $x \sim t^{1/2}$. Although this "diffusion" regime is well suited to the intermediate stage of imbibition in long capillaries and packed beds, the LW equation fails to describe the initial stage of penetration [18].

1.6. Aim of the Study

The aim of this study is to produce porous polymeric matrices of acrylic polymers of controllable porosity and pore dimensions. A novel technique is employed for the creation of such matrices. The spheres used are synthesized by suspension polymerization of MMA and the hydrophilic nature is changed by the inclusion of 2-hydroxyethyl methacrylate (HEMA) into the formulation. The dry spheres produced at varying particle sizes and size distributions are connected to each other by an epoxy adhesive and their impregnation capacities are measured experimentally.

CHAPTER 2

EXPERIMENTAL

2.1. Materials Used

Methylmethacrylate (MMA) monomer was supplied by Birleşik Akrilik A.Ş., 2-hydroxyethylmethacrylate (HEMA) monomer and benzoyl peroxide (BPO) were the product of Merck. Polyvinylalcohol (PVA) (87% hydrolyzed, molecular weight: 85000-146000) was purchased from Aldrich.

Diglycidyl ether of bisphenol A (DGEBA) type epoxy resin (Araldite MTU), which is in liquid form, was purchased from Vantico. It is solvent free and has low viscosity at room temperature. Aliphatic amine curing agent (HY 956) in liquid form was purchased from Ciba Speciality Chemicals.

2.2. Synthesis of Polymer Microspheres

2.2.1. Synthesis of PMMA microspheres

Poly(methyl methacrylate) microspheres were synthesized by suspension polymerization of MMA monomer. The monomer was treated with aqueous NaOH to remove the inhibitor and stored in a refrigerator until use. The initiator benzoyl peroxide (BPO) (0.5 g) was dissolved in MMA (50 g) and the solution was taken into the 250 ml reactor vessel, which is equipped with a magnetic stirrer (Figure 2.1). The aqueous phase was prepared by dissolving PVA (1.5 g) in distilled water (150 ml) and added to the monomer phase. The polymerization temperature was controlled with a water bath and the polymerization reaction was carried out at 85^0C for 5 hours at the stirring rates of 400, 700 and 900 rpm. After completion of the reaction, the microspheres were filtered and washed with distilled water and methanol several times and dried at 60^0C under vacuum for 24 hours.

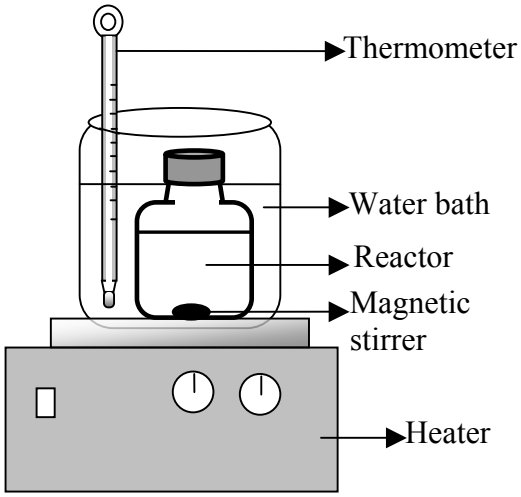

Figure 2.1. Experimental set-up for suspension polymerization

2.2.2. Synthesis of Poly(MMA-HEMA) microspheres

The poly(methylmethacrylate-2-hydroxyethylmethacrylate) microspheres were produced by suspension polymerization of MMA and HEMA (with 2 different HEMA contents; 5% and 15 % in weight). The polymerization procedure was the same as the preparation of PMMA microspheres except the monomer composition and the stirring rate. The copolymerization reaction was carried out at only one stirring rate; 900 rpm.

2.3 Characterization of Polymer Microspheres

2.3.1. ^{1}H-Nuclear Magnetic Resonance (NMR)

A Bruker 400 MHz NMR spectrometer was used to characterize the polymer samples. For NMR spectra, 5-10 wt % solutions of polymer in deuterated chloroform were prepared with the help of an ultrasonic stirrer, then the spectrum of the samples were taken.

2.3.2. Particle Size Analysis

The particle size distributions of the microspheres were determined using a Malvern Master Sizer particle size analyzer, which functions under the principle of laser diffraction. The size distribution curve displays the particle size along the x-axis and the percentage along the y-axis. From these data the average mean diameter of the microspheres was determined.

2.3.3. Scanning Electron Microscope (SEM)

Morphological studies were carried out on manually fractured surfaces of polymer samples at various magnifications, after gold plating by using scanning electron microscope, JEOL, JSM-6400.

2.4. Surface Energy Measurements

The surface energies of pure PMMA and poly(MMA-HEMA) copolymers were calculated by using tensiometry method. In this method, the solid sample was brought to contact with the probe liquids and the force applied to the sample was recorded in terms of weight change. In order to prepare the specimens, the polymer microspheres were transformed into thin films by compression in hot press and the produced thin films were cut in rectangular shape.

Contact angle measurements were performed by use of an electronic microbalance (Sartorius microbalance model M25 D) and a motor mike (vertical mobile stage; Oriel model 18008). A schematic view of the contact angle apparatus is presented in Figure 2.2.

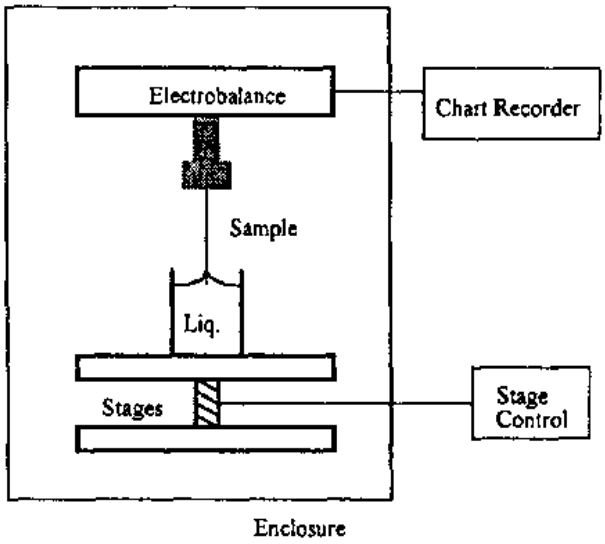

Figure 2.2. Contact angle apparatus set-up

In the surface energy experiments, diiodomethane (DIM) was used as the probe liquid for the Lifshitz-van der Waals interactions while ethylene glycol (EG), and formamide (FA) were used for the acid-base interactions. In addition, *n*-decane was used as a completely wetting liquid to determine the perimeters of the specimens. The analytical grade liquids were used as supplied. Properties of the probe liquids used are represented in Table 2.1.

Table 2.1. Surface free energies (mN m^{-1}) for the probe liquids used, at 20 ^{0}C [9].

Liquid	γ^T	γ^{LW}	γ^{AB}	γ^a	γ^b
n-Decane	23.83	23.83	-	-	-
Diiodomethane	50.80	50.80	-	-	-
Formamide	58.00	39.00	19.00	2.28	39.60
Ethylene glycol	48.00	29.00	19.00	1.92	47.00

2.5. Sample Preparation for the Analysis of Capillary Impregnation and Volumetric Flow Rate

For capillary impregnation and volumetric flow rate experiments, samples were prepared in cylindrical shapes. First a 5% (wt) epoxy solution was prepared by dissolving epoxy and hardener (with 5/1 mixing ratio) in diethylether. 2.7 ml of the epoxy solution was poured on the polymer beads weighed as 5 g. After mixing the dense solution for a short time, it was taken into a cylindrical glass pipe with the internal diameter of 18 mm and the mixture was compressed with a plastic rod and kept at 75^0C for 3 hours for curing. Finally the cured sample was cut from its ends for a smooth surface.

2.6. Density Measurements and Pore Volumes

Apparent densities and pore volumes of the samples, prepared for the measurements of capillary impregnation and volumetric flow rate, were calculated simply by using their volumes and masses. A micrometer was used to measure the dimensions of the samples.

2.7. Measurement of Volumetric Flow Rate

For the volumetric flow rate measurements at different pressures, a metal pipe, which has the diameter of 6 cm and the length of 105 cm, was used. The cylindrical sample was adhered into a plastic hose and the hose was bonded to the metal pipe. The pipe was filled with water and connected to a nitrogen supply (Figure 2.3). After the pressure was adjusted to desired value, the tap was opened and water coming through the sample was collected for 5 minutes. This

experiment was performed with 3 different particle sizes; 45, 55 and 112 μm and 3 different pressures; 1, 2 and 3 bars.

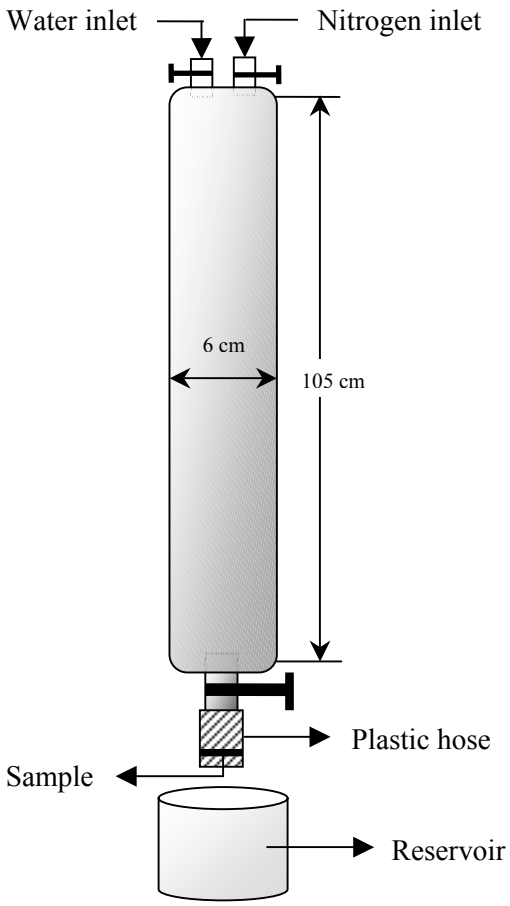

Figure 2.3. Experimental set-up for volumetric flow rate measurement

2.8. Measurement of Capillary Impregnation

Impregnation of water through porous structures of PMMA with different pore sizes and of poly(MMA-HEMA) with different HEMA contents was measured. In order to estimate the effect of pore size on the capillary impregnation, the samples were prepared with PMMA beads having 3 different

particle sizes (45, 55 and 112 μm) and to observe the effect of HEMA content, poly(MMA-HEMA) beads (~45μm), having 5% and 15% HEMA contents, were used.

An evaporating dish was filled with distilled water and placed on a balance. The sample was hung with a metal rod over the water. The balance was lifted by the help of a motor mike (vertical mobile stage) until the sample touches water surface and the data was collected in terms of weight change at every 5 seconds. The equipment used in this study is shown in Figure 2.4.

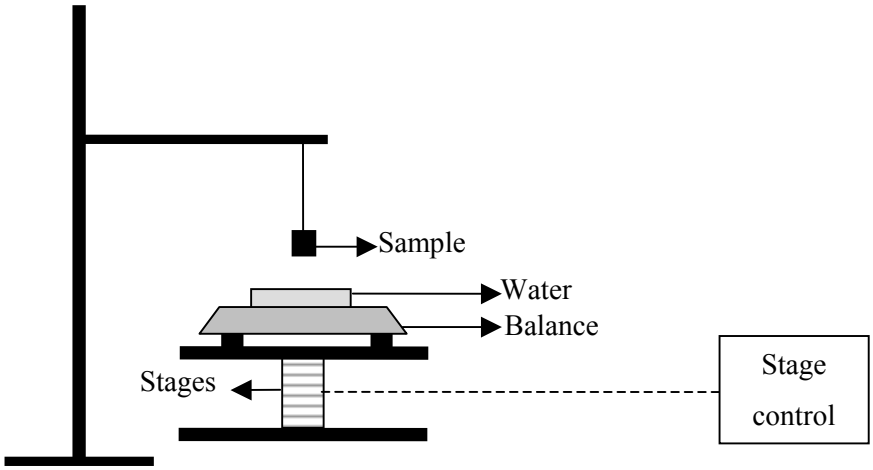

Figure 2.4. Experimental set-up for capillary impregnation measurement

2.9. Charpy Impact Tests

Charpy impact tests (unnotched) were conducted by Pendulum Impact Tester of Coesfeld Material Test machine. The test specimens were prepared with PMMA beads having 3 different particle sizes (45, 55 and 112 μm), and poly(MMA-HEMA) beads with 5% and 15% HEMA contents. All the samples were prepared with epoxy solutions having 2 different epoxy contents (5% and

10% in weight). In addition, the specimens were aged in water for 30 days prior to impact tests. The method used for specimen preparation was the same as sample preparation for the analysis of capillary impregnation and volumetric flow rate, however in that case a bar-shaped mould having dimensions of 10x10x50 mm was used.

CHAPTER 3

RESULTS AND DISCUSSION

3.1. ^{1}H-Nuclear Magnetic Resonance (NMR)

The monomers and synthesized polymers were identified by ^{1}H-NMR and the spectra are given in Figure 3.1 to Figure 3.5.

In the ^{1}H-NMR spectrum of MMA (Figure 3.1) four singlet peaks were observed. The assigned protons are shown in molecular formula of the monomer and the corresponding chemical shifts in Table 3.1.

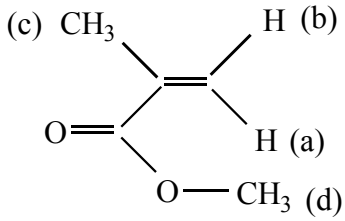

Table 3.1. Chemical shifts (ppm) for the protons of MMA

Proton type	Shift (ppm)	Group
H (Ha)	6.05	Ethylene (cis)
H (Hb)	5.58	Ethylene (trans)
CH_3 (Hc)	1.93	Methyl
CH_3 (Hd)	3.67	Ester

Figure 3.2 shows the ^{1}H-NMR spectrum of HEMA. The assigned protons of HEMA are shown in the molecular formula and Table 3.2 represents the chemical shifts of the protons.

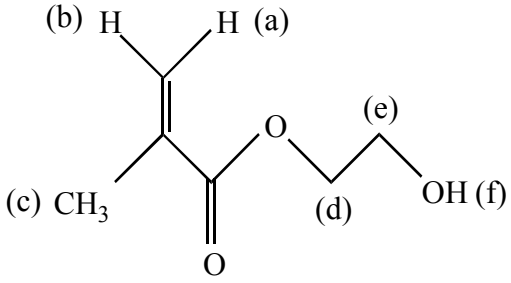

Table 3.2. Chemical shifts (ppm) for the protons of HEMA

Proton type	Shift (ppm)	Group
H (Ha)	6.05	Ethylene (cis)
H (Hb)	5.58	Ethylene (trans)
CH_3 (Hc)	1.93	Methyl
CH_2 (Hd)	4.20	Ester
CH_2 (He)	3.81	Ester
OH (Hf)	2.57	Alcohol

The ^{1}H-NMR spectrum of PMMA is shown in Figure 3.3. The peaks for vinyl groups are not observed and methylene peaks appeared in the range of 1.2-2 ppm, which clearly shows that polymerization proceeds via opening of vinyl groups. PMMA has three types of hydrogen atoms; three equivalent α-methyl hydrogens, three equivalent ester methyl hydrogens, and two β- methylene hydrogens. The ester methyl hydrogens, being equivalent and having no close neighbours, form a singlet at 3.6 ppm. The environment of two methylene hydrogens changes with tacticity. In the syndiotactic arrangement the two geminal methylene protons are in equivalent environments; they have the same chemical shift and should appear in the spectrum as a singlet. In the isotactic arrangement, since the two protons are in different environments, they should have different chemical shifts and should mutually split, producing two doublets in the spectrum. For the atactic arrangement, identification of methylene and methyl protons is more complicated, the peaks are broad and have some bands due to different chemical shifts. Therefore, we concluded that our polymers are atactic.

In the ^{1}H-NMR spectra of poly(MMA-HEMA) copolymers (Figure 3.4 and Figure 3.5), the peaks for monomeric vinyl groups are also not observed and methylene peaks appeared in the range of 1.2-2 ppm. The peak at 2.9 ppm, which is more clear for the copolymer with 15% HEMA content, corresponds for –OH group. For all the spectra there is no peak indicating the existence of residual monomer in the polymers. The peak at about 7.2 ppm is due to impurity of the solvent deuterated chloroform.

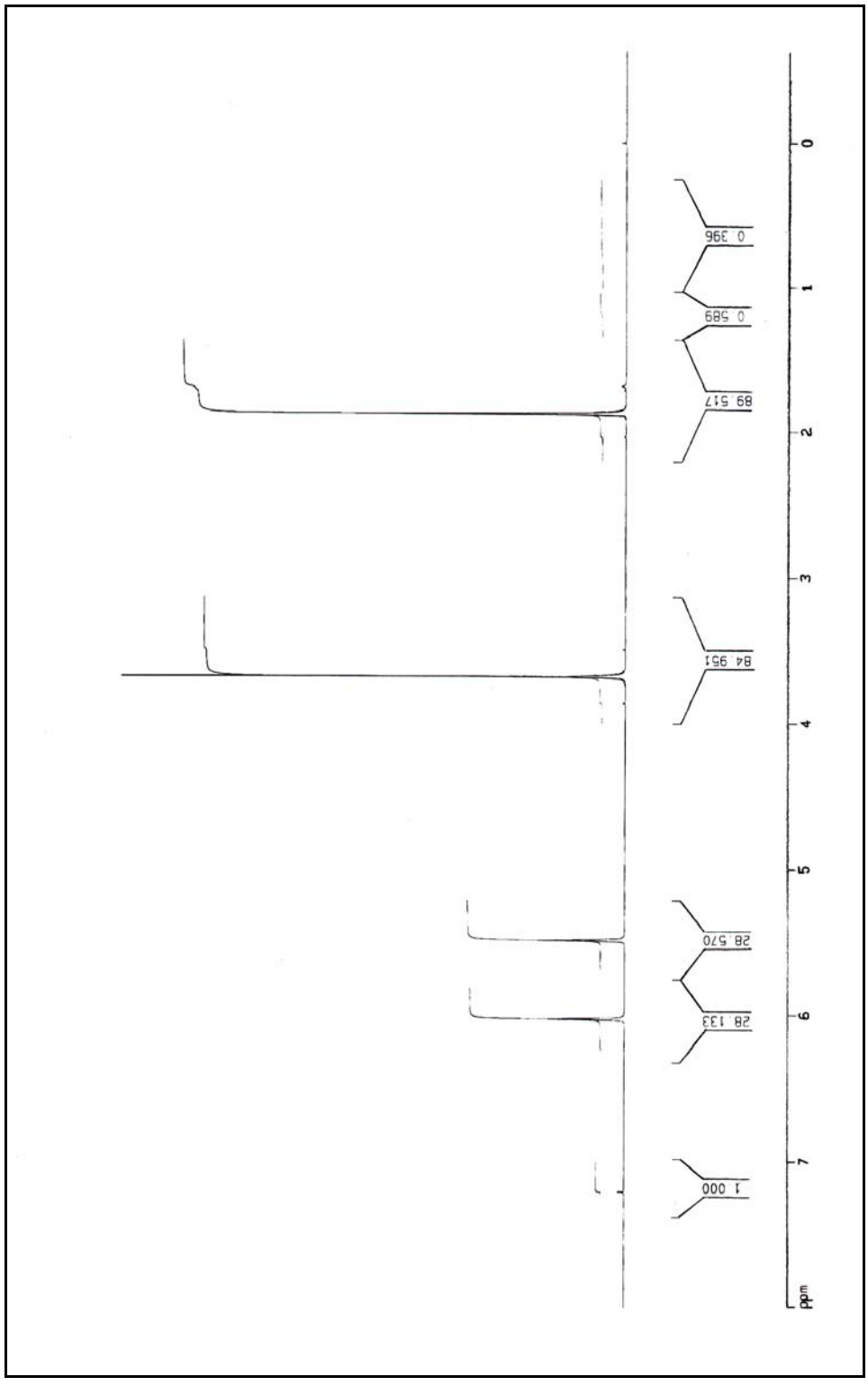

Figure 3.1. ^{1}H-NMR spectrum of MMA

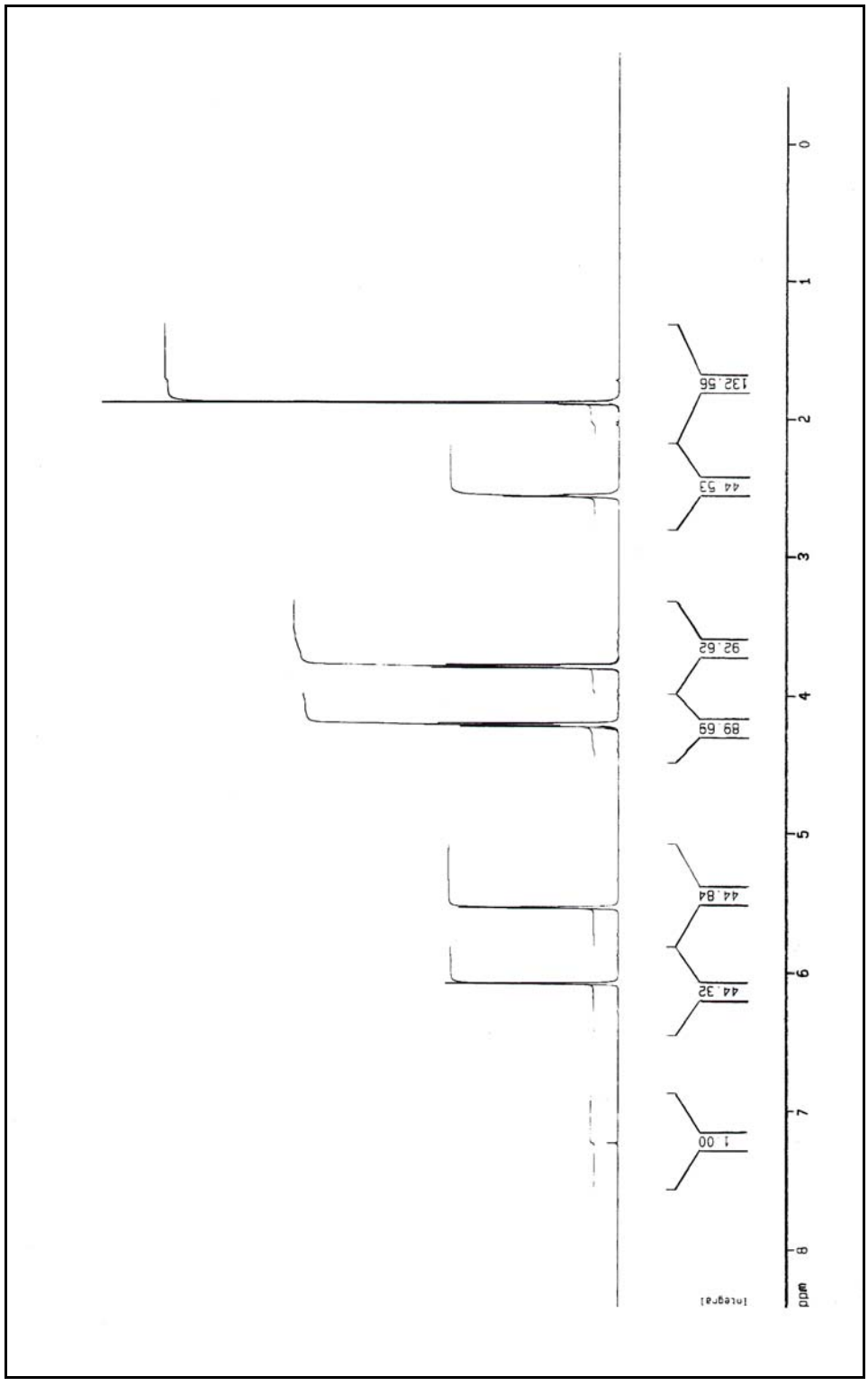

Figure 3.2. ^{1}H-NMR spectrum of HEMA

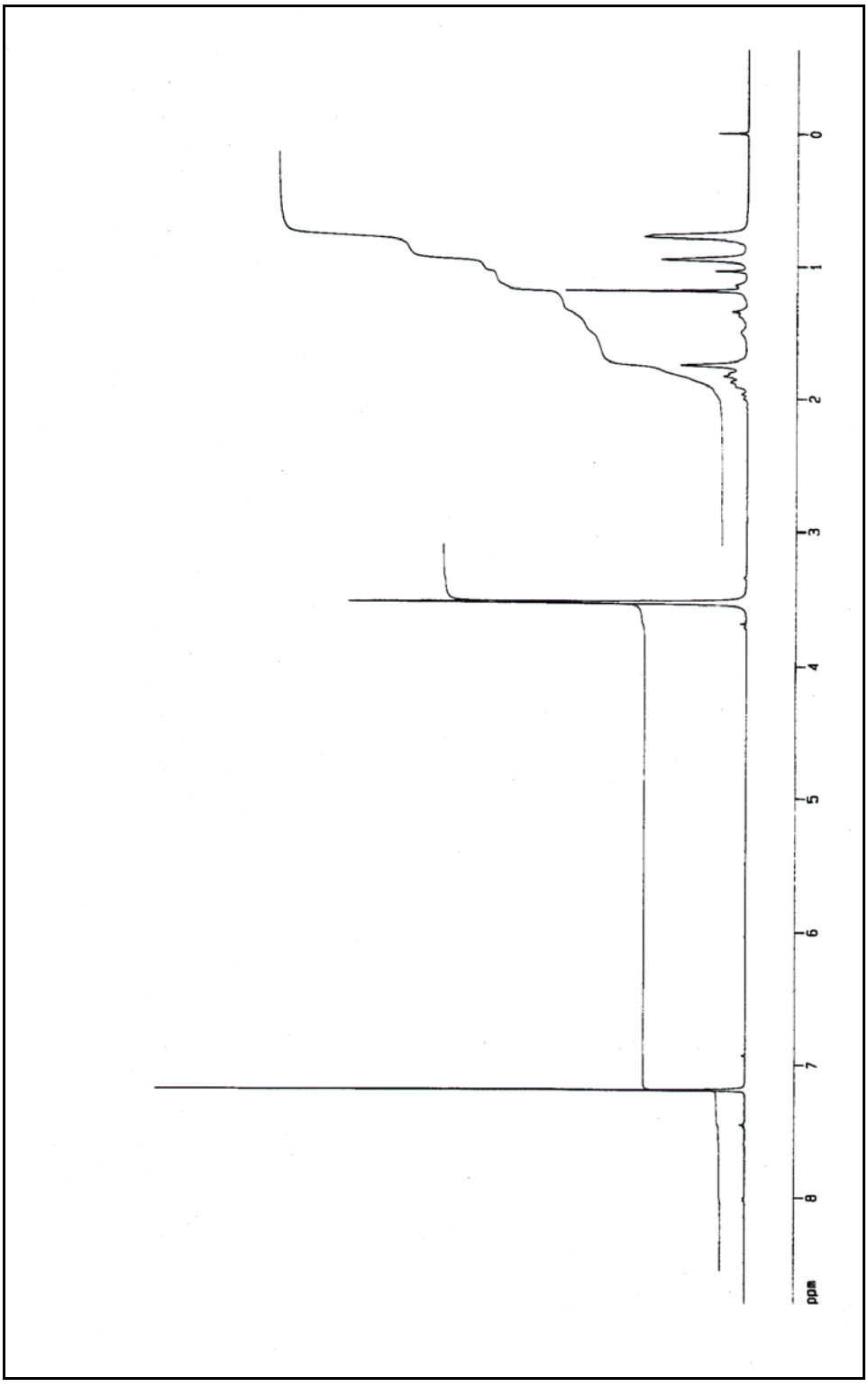

Figure 3.3. ^{1}H-NMR spectrum of PMMA

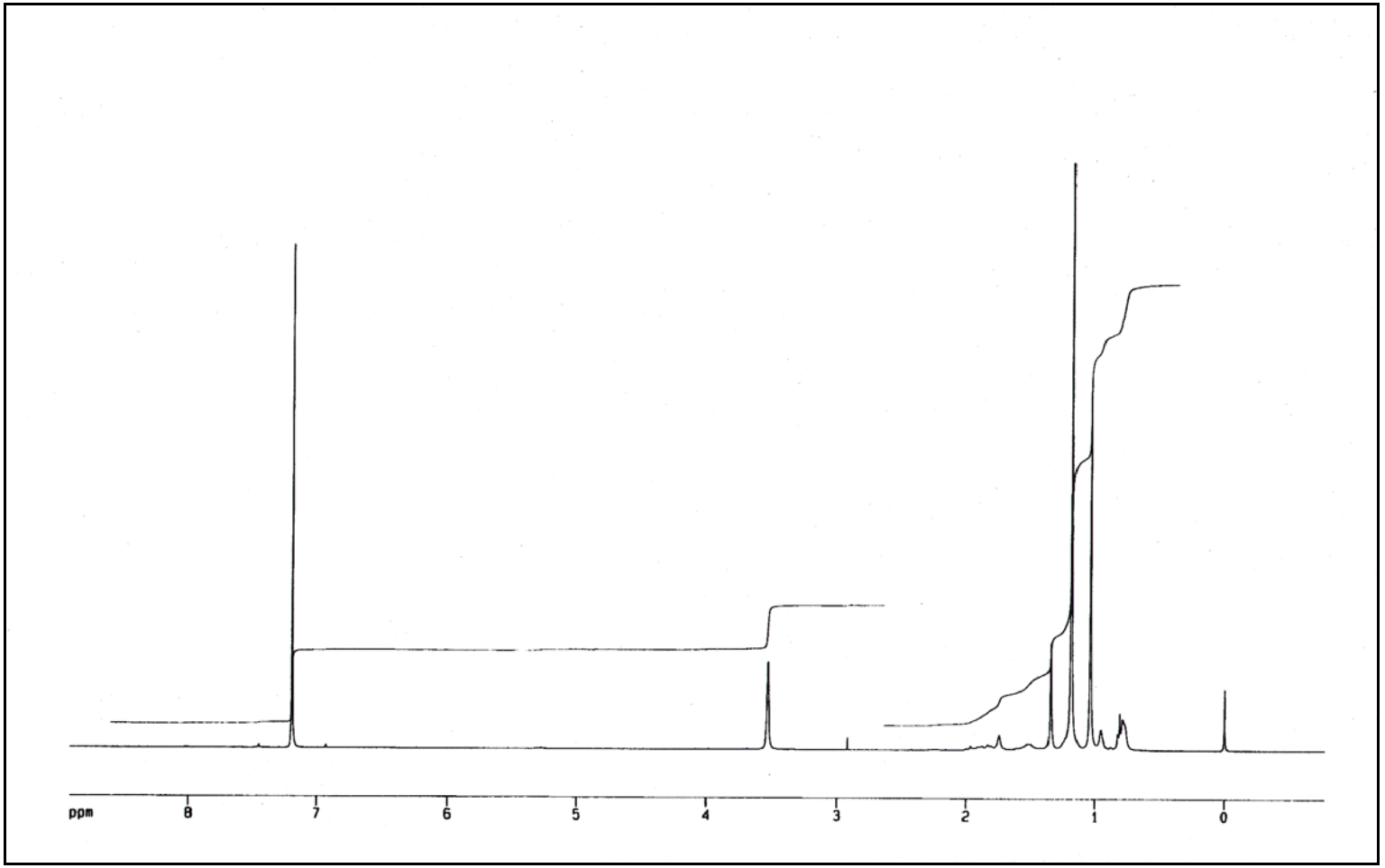

Figure 3.4. ^{1}H-NMR spectrum of poly(MMA-HEMA) copolymer with 5% HEMA content

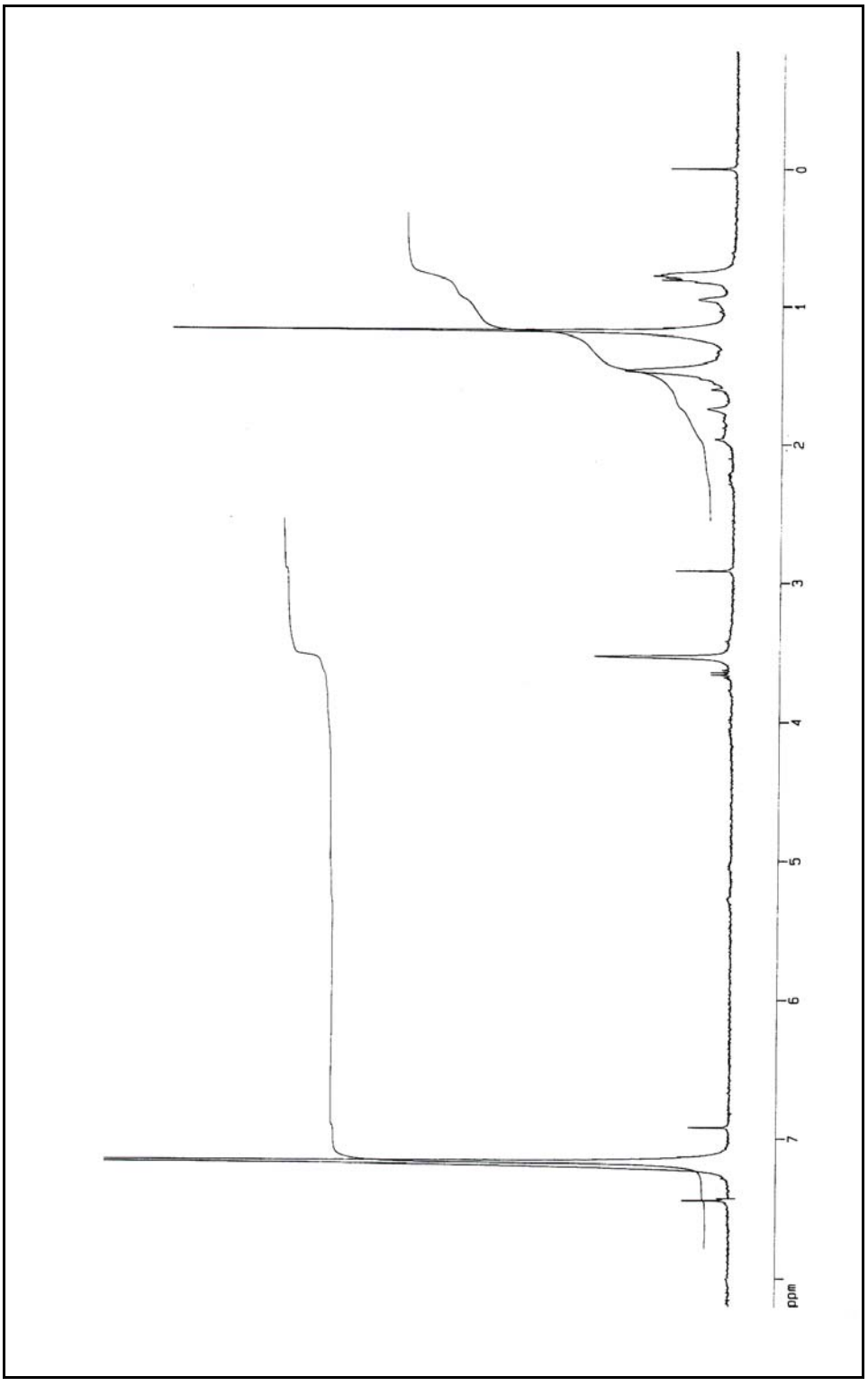

Figure 3.5. ^{1}H-NMR spectrum of poly(MMA-HEMA) copolymer with 15% HEMA content

3.2. Particle Size Analysis of Microspheres

Particle size distribution curves of the microspheres are given in Figures 3.6 to 3.10 and the results are shown in Table 3.3.

Experimental parameters employed for microsphere preparation (speed of mixing, stabilizer concentration, initiator concentration etc.) affect the particle size of the synthesized microspheres. In this study, the microspheres were prepared at the stirring rates of 400, 700 and 900 rpm. However, poly(MMA-HEMA) copolymerization was performed only at 900 rpm stirring rate. Except stirring rate, all the other parameters were the same for all of the experiments.

The volume mean diameters (VMD) of the synthesized microspheres were as follows: For 400, 700 and 900 rpm stirring rates, the volume mean diameters of the PMMA microspheres were 111.69, 55.23 and 45.12 μm respectively. For 900 rpm stirring rate, poly(MMA-HEMA) copolymers, having 5% and 15% HEMA contents, had the mean particle diameters of 48.37 and 47.46 μm respectively.

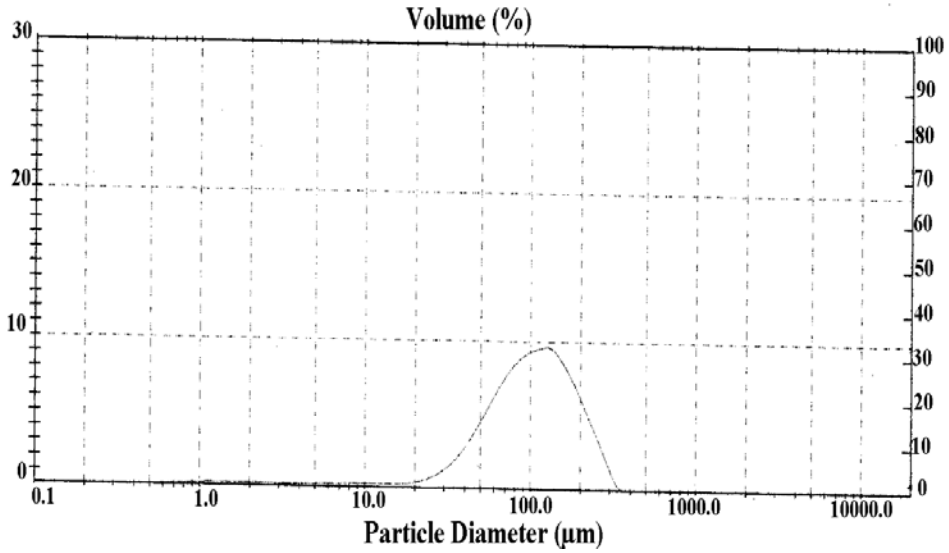

Figure 3.6. Particle size distribution curve for PMMA microspheres prepared with 400 rpm stirring rate.

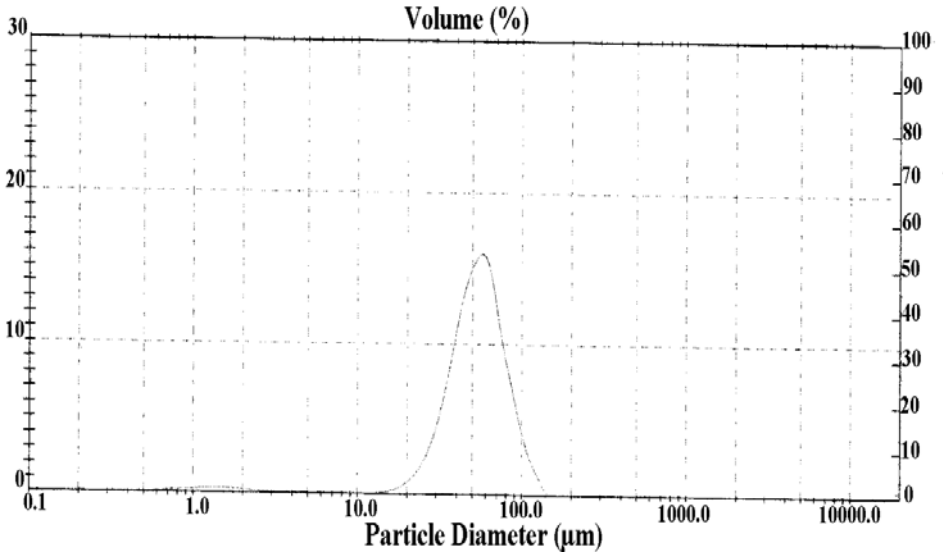

Figure 3.7. Particle size distribution curve for PMMA microspheres prepared with 700 rpm stirring rate.

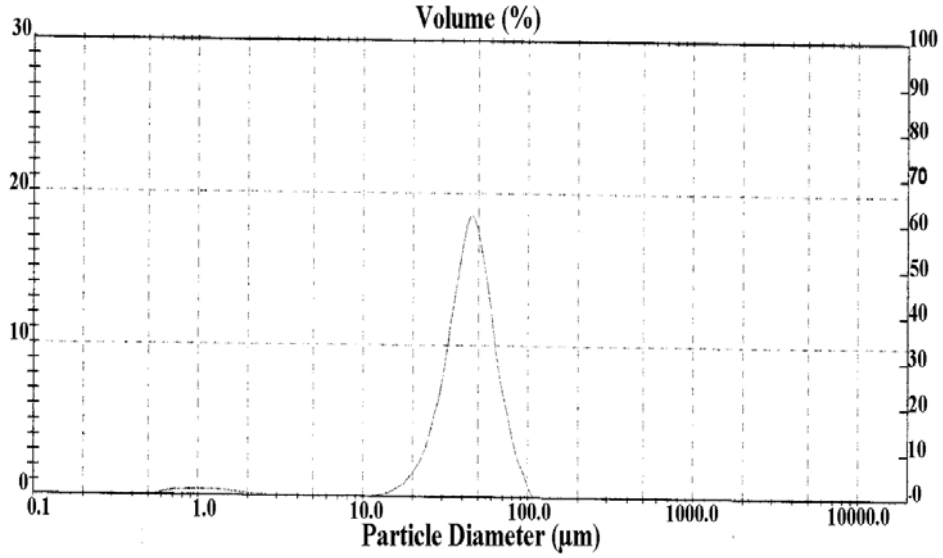

Figure 3.8. Particle size distribution curve for PMMA microspheres prepared with 900 rpm stirring rate.

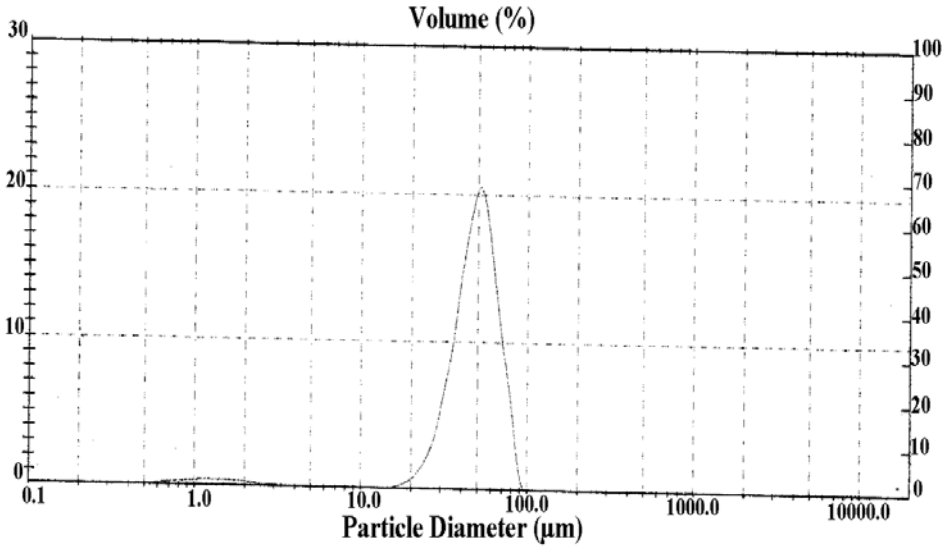

Figure 3.9. Particle size distribution curve for poly(MMA-HEMA) (5% HEMA content) microspheres prepared with 900 rpm stirring rate.

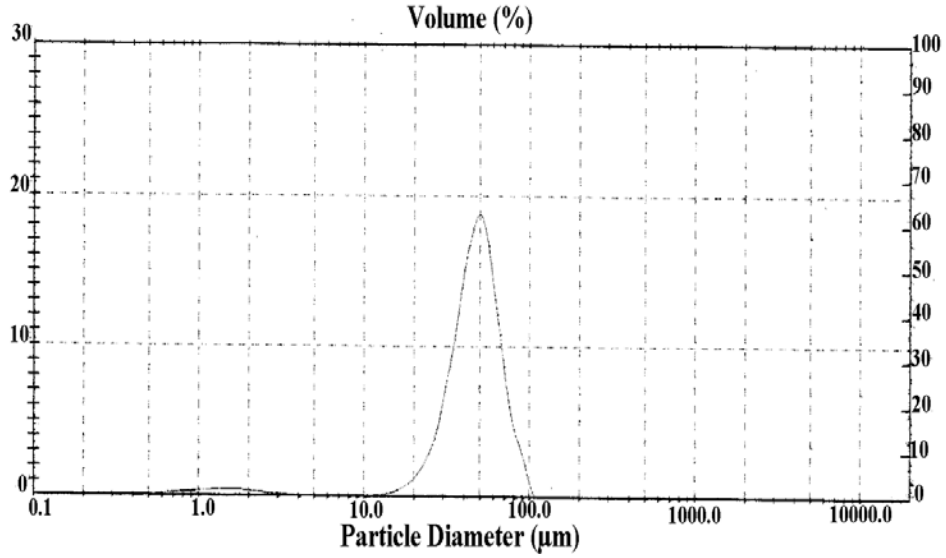

Figure 3.10. Particle size distribution curve for poly(MMA-HEMA) (15% HEMA content) microspheres prepared with 900 rpm stirring rate.

Table 3.3. Particle size analysis results

Microsphere type	Stirring rate	D(v,0.1) (μm)	D(v,0.5) (μm)	D(v,0.9) (μm)	D(4,3) (μm)	D(3,2) (μm)
PMMA	400	37.84	100.66	204.76	111.69	30.30
PMMA	700	29.59	53.29	85.52	55.23	22.14
PMMA	900	25.75	44.20	67.35	45.12	17.92
P(MMA-HEMA) (5% HEMA)	900	29.77	48.61	69.27	48.37	19.54
P(MMA-HEMA) (15% HEMA)	900	27.17	46.98	69.97	47.46	19.67

D(v,0.1) is the size of particle for which 10% of the sample is below this size.
D(v,0.5) is the size of particle at which 50% of the sample is smaller and 50% is larger than this size. This value is also known as the mass median diameter (MMD).
D(v,0.9) gives a size of particle which 90% of the sample is below this size.
D(4,3) is the volume mean diameter (VMD).
D(3,2) is the surface area mean diameter (SMD) also known as the Sauter mean.

3.3. Surface Energies

The total surface energy (γ) of a given non-metallic material (i) can be considered as being composed of two parts, namely, the Lifshitz-van der Waals (γ_i^{LW}) component and the acid-base (γ_i^{AB}) component (equation (11)). In equation (12), γ_i^a and γ_i^b are the independent Lewis acid and Lewis base components of the surface free energy.

$$\gamma_i^{TOT} = \gamma_i^{LW} + \gamma_i^{AB} \qquad (11)$$

$$\gamma_i^{AB} = 2\,(\gamma_i^a\ \gamma_i^b)^{1/2} \qquad (12)$$

A characteristic feature of the Lewis acid and base components is their non-additivity. Hence if phase (i) possesses only γ_i^a or γ_i^b , this component does not participate in the total surface free energy of the phase (i). However it will interact with the complementary component of phase (j).

For a bipolar liquid (L), with surface tension γ_L, acidic (γ_L^a) and basic (γ_L^b) surface parameters, and an apolar surface component γ_L^{LW}, the complete equation to be considered is as follows;

$$(1+\cos\theta_L)\,\gamma_L^{TOT} = 2[(\gamma_L^{LW}\gamma_S^{LW})^{1/2} + (\gamma_L^a\,\gamma_S^b)^{1/2} + (\gamma_L^b\,\gamma_S^a)^{1/2}] \qquad (13)$$

which can be constructed to form a set of two simultaneous equations, in terms of the parameters of the solid γ_S^a, γ_S^b and two advancing contact angles θ_1 and θ_2, which are measured on the solid surface. These two equations can then be simultaneously solved for γ_S^a and γ_S^b provided that γ_i^a, γ_i^b and γ_L^{LW} for the probe liquids are known [11].

The probe liquids used in this study and their properties are given in Table 2.1. The cosθ for each combination of the three polymer and the three test liquids are given in Table 3.4. These data were used in the calculation of surface free energies of the polymers.

Table 3.4. Contact angle (θ) values of the PMMA and poly(MMA-HEMA) copolymers determined with three test liquids

Polymer	Diiodomethane	Ethylene glycol	Formamide
PMMA	50.9	63.9	63.3
poly(MMA-HEMA) (5% HEMA)	48.7	62.6	59.3
poly(MMA-HEMA) (15% HEMA)	46.4	51.7	55.2

The results of the surface energy measurements are presented in Table 3.5 together with the calculated surface energy components.

Table 3.5. Calculated surface energies (mN m^{-1}) for the polymers

Polymer	γ^{LW}	γ^{a}	γ^{b}	γ^{TOT}
PMMA	33.74	0	10.10	33.74
poly(MMA-HEMA) (5% HEMA)	34.99	0	12.92	34.99
poly(MMA-HEMA) (15% HEMA)	36.27	0	24.52	36.27

Surface tension which is a measurement of surface energy is the property, due to molecular forces, by which all liquids through contraction of the surface tend to bring the contained volume onto a shape having the least surface area. Wettability is the ability of solids to retain liquids on their surface and it is quantitatively described by the angle, which forms the surface of the liquid drop with the substrate in the contact point. This angle θ only depends on the surface energies of the liquid and solid substrate. The higher the surface energy of the solid substrate, the better wettability it will have.

In order to determine the wettability properties of the polymers, the contact angles between water and the polymers were measured. The measured contact angles are given in Table 3.6.

Table 3.6. Contact angles (θ) between water and the polymers

Polymer	**θ**
PMMA	73.09
5% HEMA	71.83
15% HEMA	69.44

3.4. Density measurements and Pore Volumes

Apparent (or bulk) density is the mass of particles per unit volume of the bed and it is directly proportional to porosity (ϕ), which is the space not occupied by particulate material and expressed as a percentage of the total volume of the bed.

Density method is one of the various experimental methods used to determine the porosities of porous materials. This method depends on determining the bulk density of the sample and the density of the solids in the sample. Since the mass of a porous medium resides entirely in the solids matrix, we have the following:

$$m = \rho_s V_s = \rho_b V_b \qquad (14)$$

where m is the mass of the sample, V_s and ρ_s are the volume and the density of the solids in the sample, V_b and ρ_b are the bulk volume and the bulk density of the sample.

By the definition of porosity $\phi = 1-(V_S / V_B) = 1-(\rho_S / \rho_B)$
The density method yields total porosity [3].

The calculated apparent densities and pore volumes of the cylindrical porous PMMA samples, prepared with 5% and 10% epoxy solutions, are represented in Table 3.7. For the calculations, the density of PMMA beads was taken as 1.18 g/cm^3, which was found by the help of a pycnometer, and the densities of epoxy resin and curing agent were taken as 1.1 g/cm^3 and 1.05 g/cm^3 respectively.

Table 3.7. Apparent densities and pore volumes of porous PMMA samples

VMD (μm) of microspheres used	**Epoxy content of the soln. (% wt.)**	**Apparent density (g/cm^3) (±0.001)**	**Pore Volume (%) (±0.2)**
45	5	0.746	36.8
55	5	0.746	36.8
112	5	0.747	36.8
45	10	0.792	32.9
55	10	0.800	32.2
112	10	0.819	30.6

The porosities of the samples, prepared with 3 different mean particle diameter, are almost the same for the same epoxy content of the solution used in the preparation. Since the particle size distribution broadens with the increasing mean particle diameter (Figures 3.6 to 3.8), there is not a considerable difference between the porosities. The porosities of the samples decreased by nearly 5%, when the solution used has 10% epoxy content. At 400 rpm stirrer speed with 112 μm volume mean particle diameter the polydispersity of the powder is apparent in Figure 3.6., hence, the porosity of this sample is lower than the others.

3.5. Volumetric Flow Rate

Volumetric flow rate measurements were performed on samples prepared with PMMA beads having mean particle diameters of 45, 55 and 112 μm. The epoxy content of the solution used in sample preparation was 5% (w/w). These preliminary experiments were carried out to test the use of these porous matrices as mold material in ceramic production. In addition to particle diameter, the applied pressure was also variable. The permeability properties of the samples were analyzed at 3 different pressures; 1, 2 and 3 kg/cm^2, and the measured values are given in Table 3.8, in terms of volume of water passing through the porous sample per minute (cm^3/min).

If we compare the data for the same pressure, we can observe that the permeability increases as the mean particle diameter of the beads increases. In addition, it is evident that the permeability of the samples are higher at high pressures, as expected. The determining factor here is the capillary dimension together with the porosity. As capillary dimensions increase the viscous resistance decreases resulting in higher flux values.

Table 3.8. Permeability (cm^3/min) of porous PMMA samples at different pressures

Mean Particle diameters of microspheres (μm)	**Applied pressure (kg/cm^2)**	**Volume of through water per minute (cm^3/min)**
45	1	134.5
55		141.0
112		247.8
45	2	242.1
55		257.4
112		441.5
45	3	330.7
55		351.8
112		762.5

3.6. Impact Strength

Impact strength is defined as the maximum force that a material can withstand upon sudden impact without rupture and strongly dependent upon the ability of the material to move or to deform to accommodate the impact.

The Charpy impact tests were performed on the specimens prepared with PMMA and poly(MMA-HEMA) beads having different mean particle diameters and epoxy solutions with different epoxy contents. The samples were also aged in water for 30 days. Charpy impact strengths of the porous samples are given in Table 3.9.

Table 3.9. Charpy impact strengths (x 10^{-4} J/mm^2) of the porous polymer samples

Polymer	**VMD (μm) of microspheres used**	**Epoxy content of the solution (% wt.)**	**Impact strength (x 10^{-4} J/mm^2) (± 0.2)**
PMMA	45	5	2.81
	45 (aged)	5	1.96
	45	10	6.38
	45 (aged)	10	3.16
	55	5	2.71
	55 (aged)	5	1.99
	55	10	6.25
	55 (aged)	10	3.27
	112	5	2.65
	112 (aged)	5	1.83
	112	10	5.78
	112 (aged)	10	3.05
Poly(MMA-HEMA) (5% HEMA)	48	5	2.03
	48 (aged)	5	1.57
	48	10	3.17
	48 (aged)	10	2.33
Poly(MMA-HEMA) (15% HEMA)	47	5	2.24
	47 (aged)	5	1.68
	47	10	3.31
	47 (aged)	10	2.42

For the same epoxy content of the solutions, as the mean particle diameter of the microspheres increased, the impact strength slightly decreased. This was due

to the decreasing surface area of the microspheres, which results in a weaker adhesion of the beads to each other. Furthermore, there is a considerable difference between the impact strengths of specimens prepared with PMMA and poly(MMA-HEMA) copolymer beads.

As expected, increasing the amount of epoxy increased the impact strengths of the specimens which were being composed of microspheres having the same mean particle diameter. Comparing with the others without aging, the impact strengths of the aged samples decreased considerably.

3.7. Morphological Properties of Porous Polymer Samples

Morphological properties of the porous samples prepared with PMMA and poly(MMA-HEMA) copolymer beads were studied by SEM and the results are discussed by the SEM photomicrographs given in Figure 3.6 to Figure 3.25. There are two photographs for each sample; one is a general view with a lower magnification in order to see the particle size distribution and the arrangements of the microspheres, the other one is a more detailed view to observe the interactions and adhesion between the microspheres.

Figures 3.11 and 3.12 demonstrate the morphology of the porous samples prepared with PMMA microspheres, having VMD of 45 μm, and epoxy solution with 5 % epoxy content. Without filling the pores, accumulation of epoxy seen at the contacts of the beads represents the successful adhesion. As the epoxy content of the solution increased to 10 % for the same powder type, it is easier to see the epoxy resin collected at the touch points of the beads (Figures 3.13-3.14). In addition, for higher epoxy concentration, the breakage points can be observed clearly as a crater-like spot of epoxy resin on the bead surfaces.

Figures 3.15-3.18 exhibit the morphology of the samples prepared with PMMA beads having VMD of 55 μm. It is observed that the morphology is similar to that of samples with beads having VMD of 45 μm. Figure 3.18 is a good demonstration of bridge formation and resultant pore between microspheres with different sizes.

The morphological pictures of the samples composed of PMMA microspheres with VMD of 112 μm are given in Figures 3.19-3.22. From these pictures we can conclude that, unlike the others this powder type has a broad particle size distribution. Therefore, the high ratio of small microspheres (with VMD < 40μm) results in a denser packing and formation of smaller pores. This inference also approves the calculated capillary radius (by Lucas-Washburn eqn.) which was the smallest one among all the samples. Furthermore, for this sample the effect of epoxy content on the morphology is not observed clearly from the pictures.

Figures 3.23-3.26 give the SEM photographs of samples prepared with poly(MMA-HEMA) copolymer beads having 5% HEMA content and VMD of 48 μm. Comparing with the morphologies of PMMA samples, it can be concluded that the surfaces of copolymer beads are rough and adhesion is inadequate. The roughness of the copolymer beads may arise from the hydrophilic property of HEMA, which give rise to some amount of polymerization that proceeds outside the micelles.

Figures 3.27-3.30 represents the morphological properties of the samples composed of poly(MMA-HEMA) copolymer beads with 15% HEMA content and VMD of 47 μm. As it is observed, there is no such a clear distinction between the morphologies of the copolymers having 5% and 15% HEMA content.

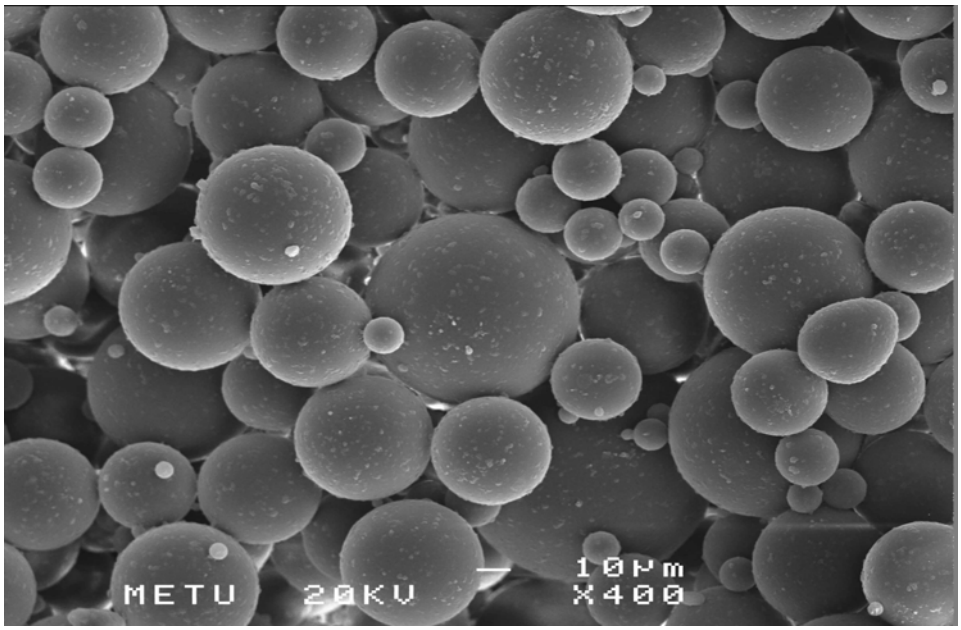

Figure 3.11. SEM photomicrograph of the sample prepared with PMMA microspheres having VMD of 45µm, and epoxy solution with 5% epoxy content. (X400)

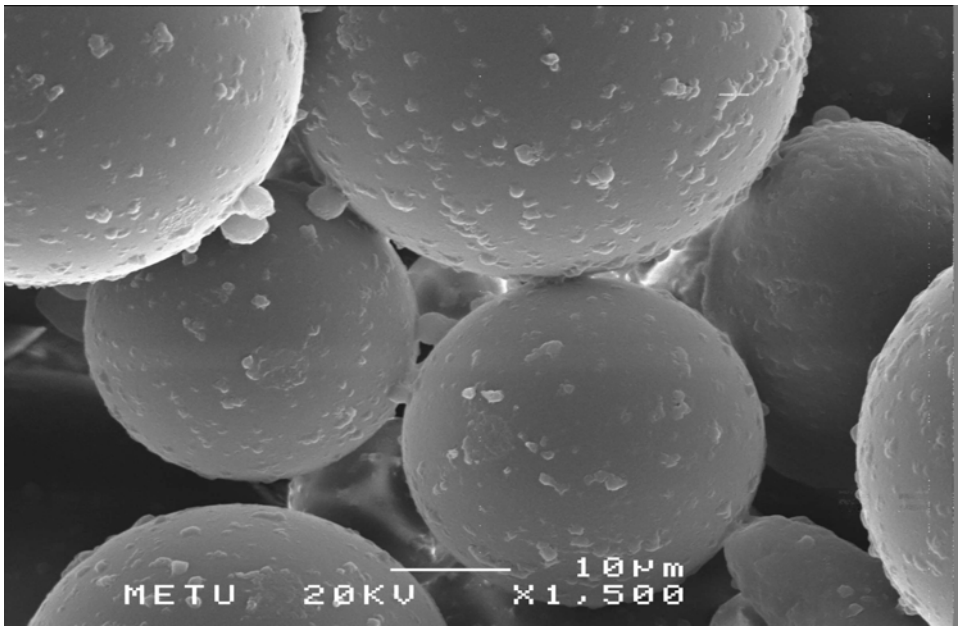

Figure 3.12. SEM photomicrograph of the sample prepared with PMMA microspheres having VMD of 45µm, and epoxy solution with 5% epoxy content. (X1500)

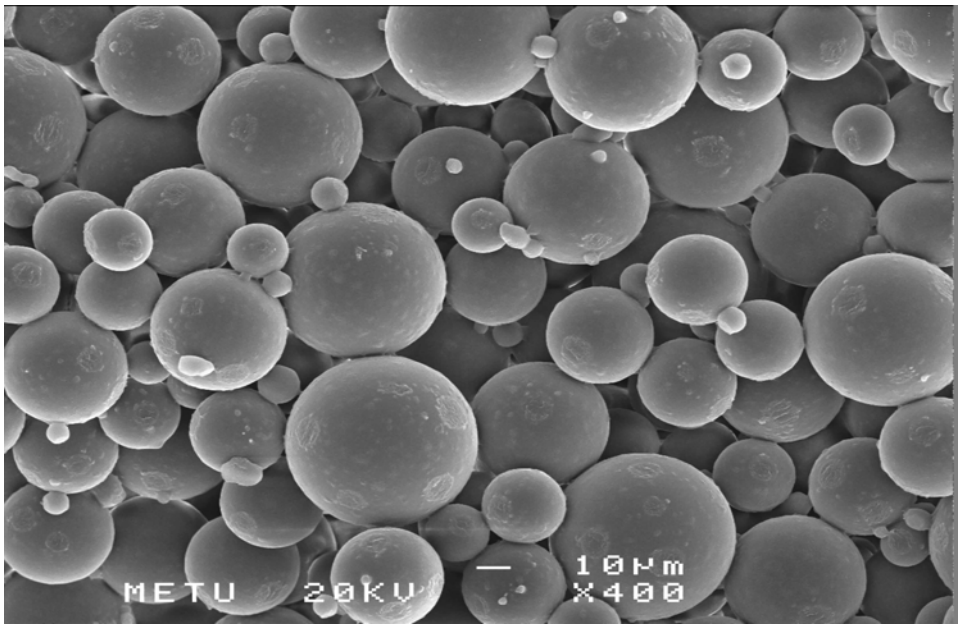

Figure 3.13. SEM photomicrograph of the sample prepared with PMMA microspheres having VMD of 45µm, and epoxy solution with 10% epoxy content. (X400)

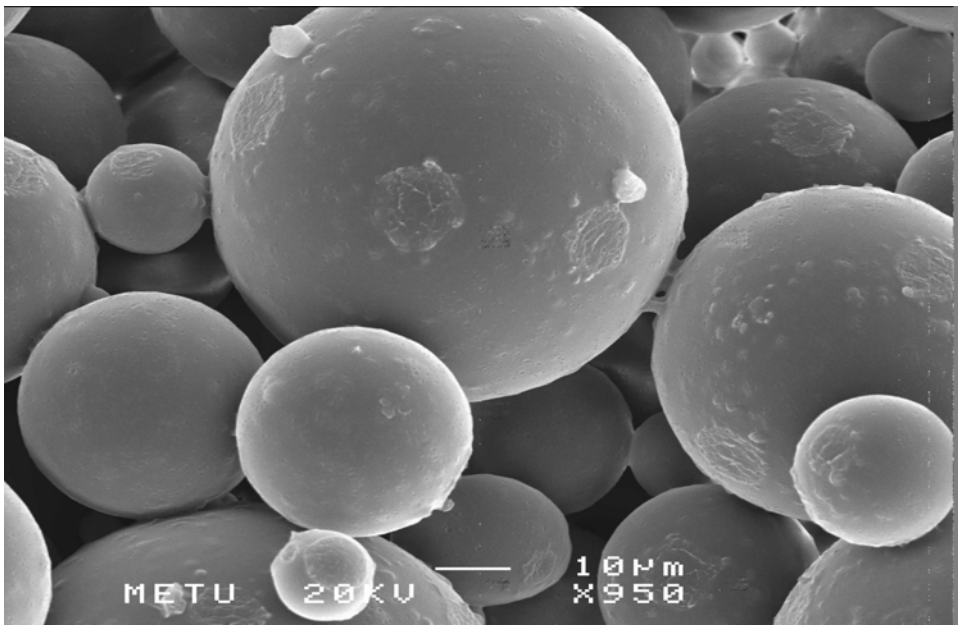

Figure 3.14. SEM photomicrograph of the sample prepared with PMMA microspheres having VMD of 45µm, and epoxy solution with 10% epoxy content. (X950)

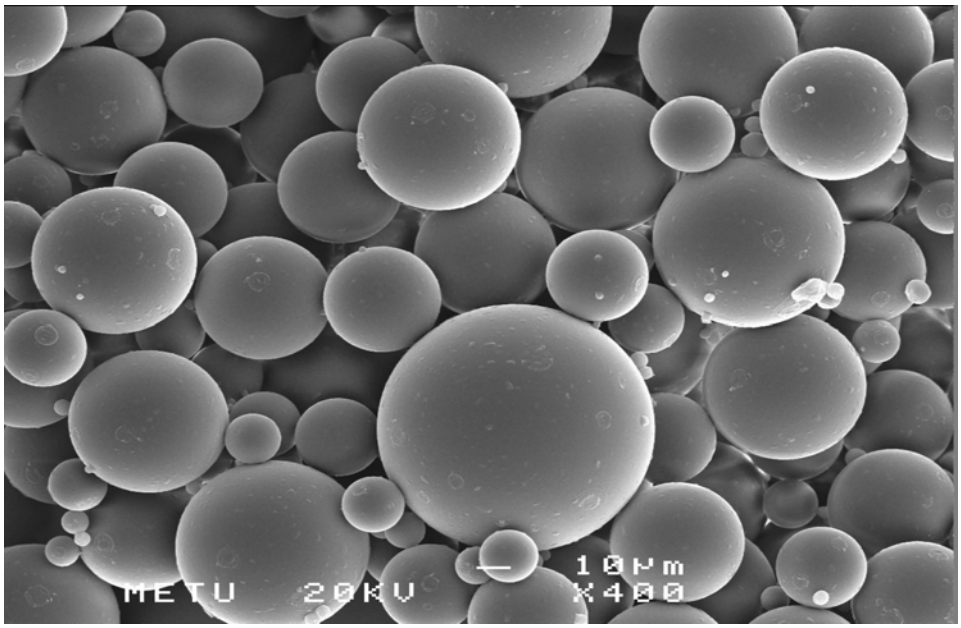

Figure 3.15. SEM photomicrograph of the sample prepared with PMMA microspheres having VMD of 55µm, and epoxy solution with 5% epoxy content. (X400)

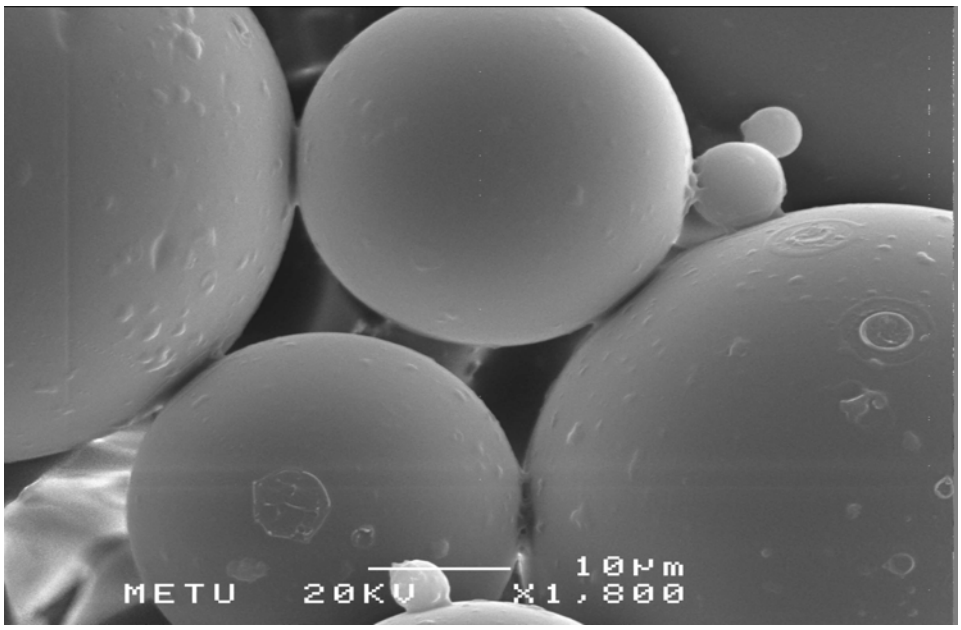

Figure 3.16. SEM photomicrograph of the sample prepared with PMMA microspheres having VMD of 55µm, and epoxy solution with 5% epoxy content. (X1800)

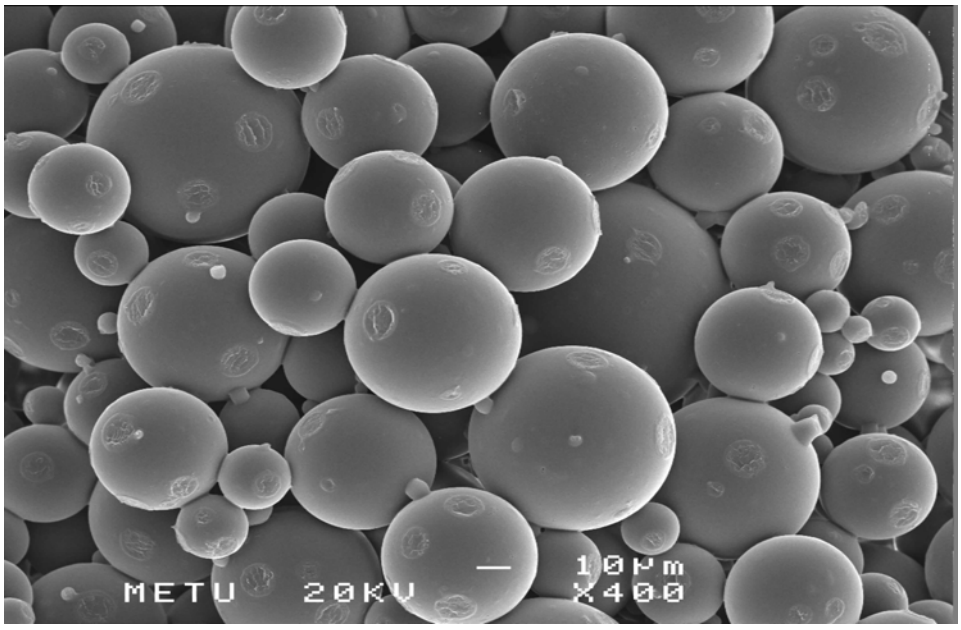

Figure 3.17. SEM photomicrograph of the sample prepared with PMMA microspheres having VMD of 55µm, and epoxy solution with 10% epoxy content. (X400)

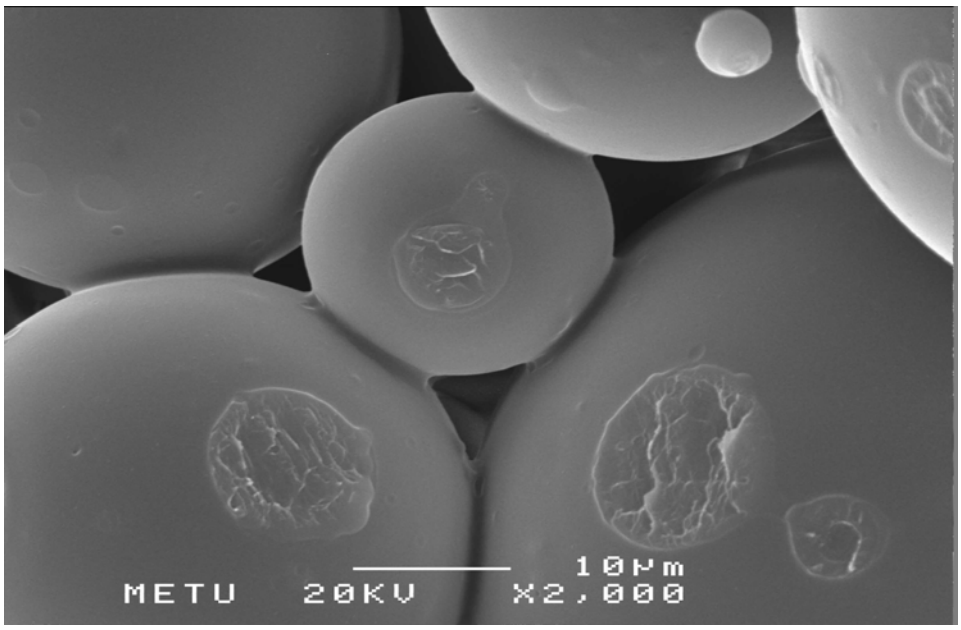

Figure 3.18. SEM photomicrograph of the sample prepared with PMMA microspheres having VMD of 55µm, and epoxy solution with 10% epoxy content. (X2000)

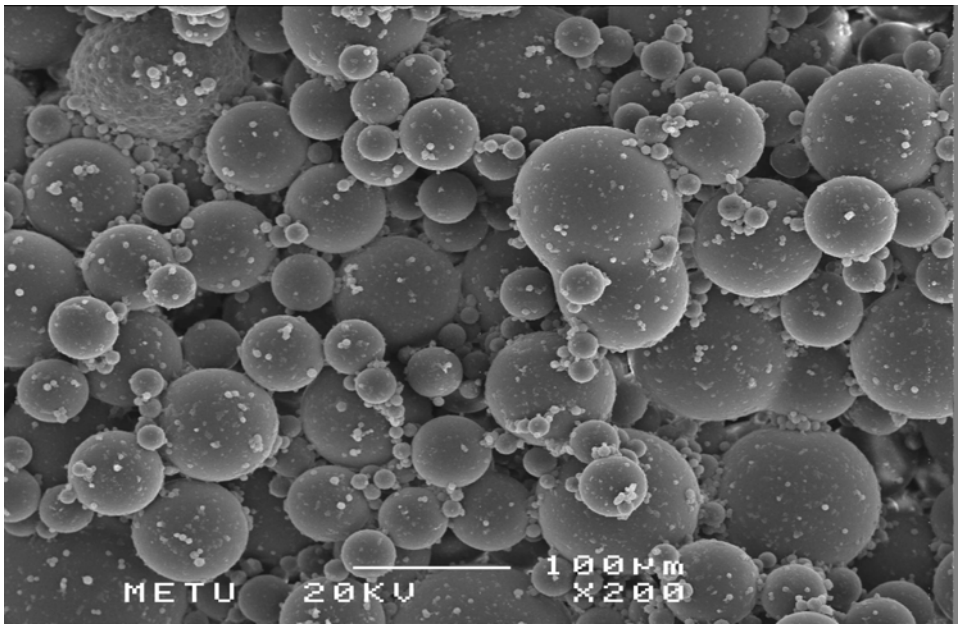

Figure 3.19. SEM photomicrograph of the sample prepared with PMMA microspheres having VMD of 112µm, and epoxy solution with 5% epoxy content. (X200)

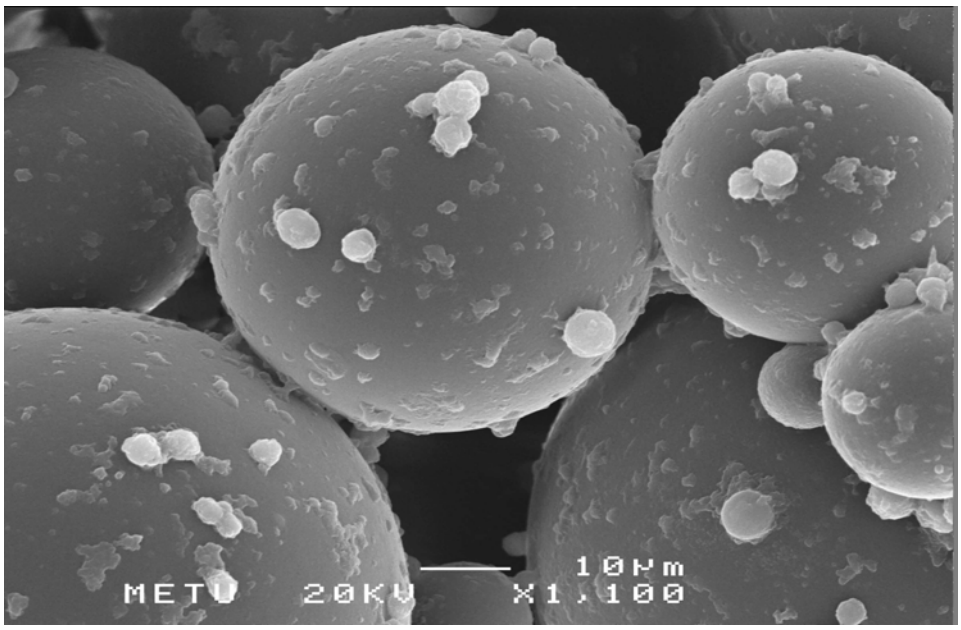

Figure 3.20. SEM photomicrograph of the sample prepared with PMMA microspheres having VMD of 112µm, and epoxy solution with 5% epoxy content. (X1100)

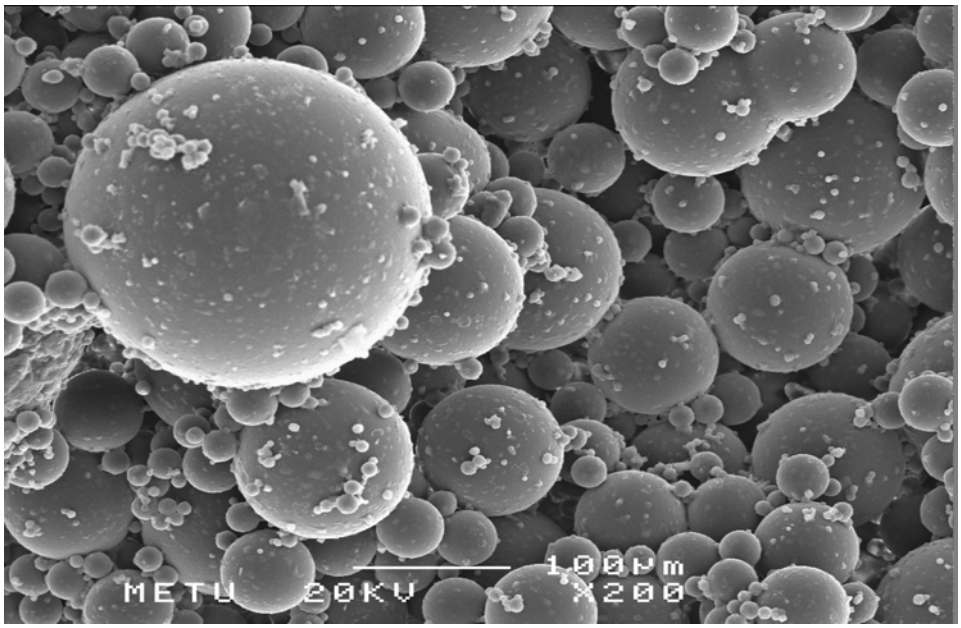

Figure 3.21. SEM photomicrograph of the sample prepared with PMMA microspheres having VMD of 112µm, and epoxy solution with 10% epoxy content. (X200)

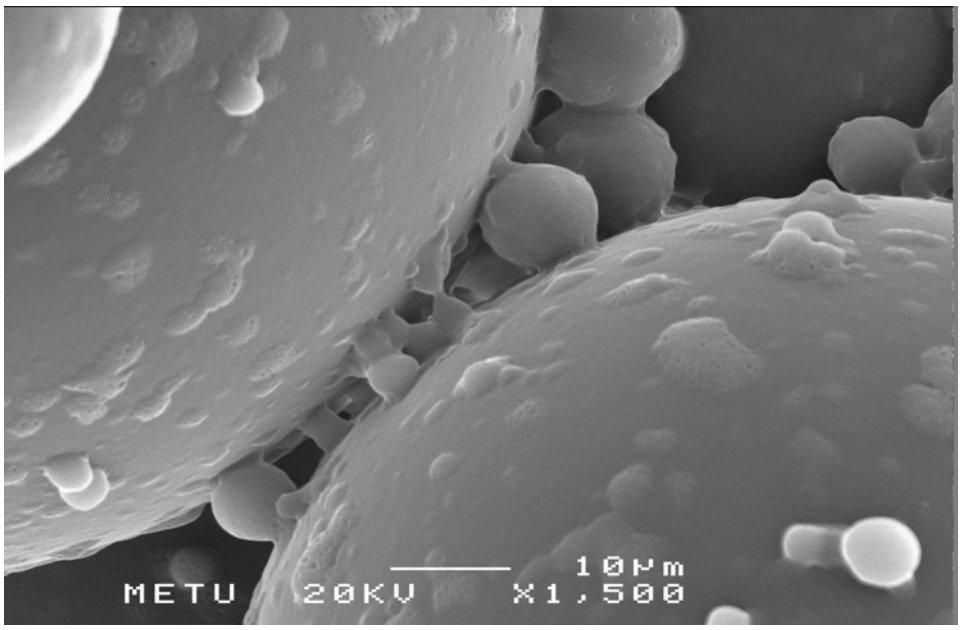

Figure 3.22. SEM photomicrograph of the sample prepared with PMMA microspheres having VMD of 112µm, and epoxy solution with 10% epoxy content. (X1500)

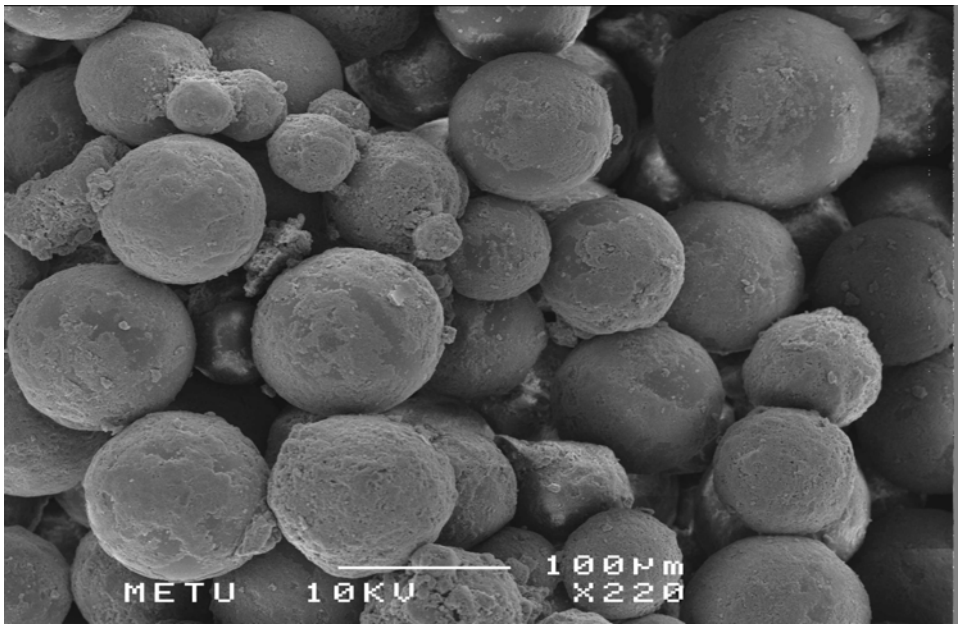

Figure 3.23. SEM photomicrograph of the sample prepared with poly(MMA-HEMA) copolymer microspheres having 5% HEMA content, VMD of 48µm, and epoxy solution with 5% epoxy content. (X220)

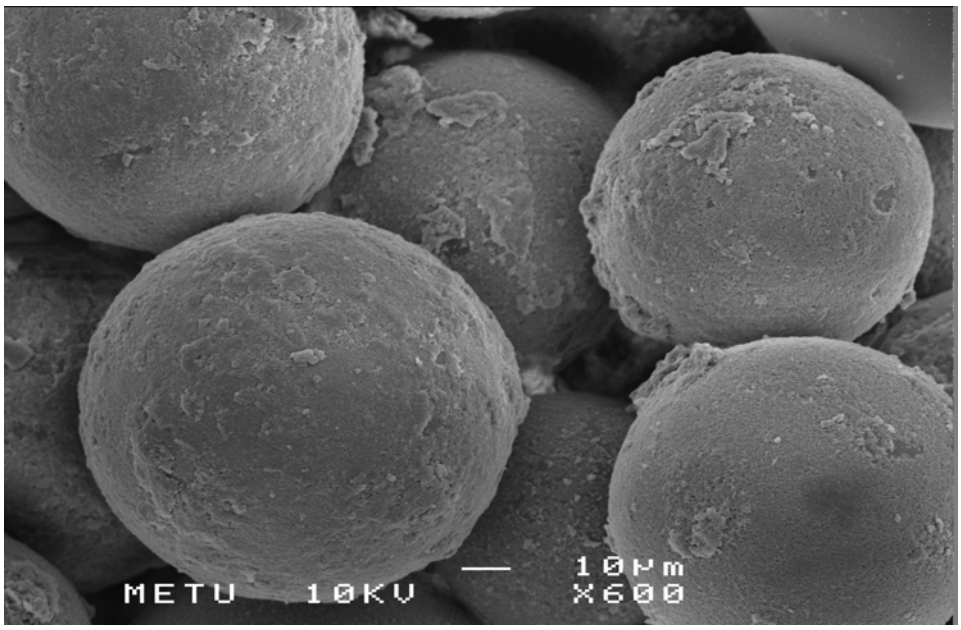

Figure 3.24. SEM photomicrograph of the sample prepared with poly(MMA-HEMA) copolymer microspheres having 5% HEMA content, VMD of 48µm, and epoxy solution with 5% epoxy content. (X600)

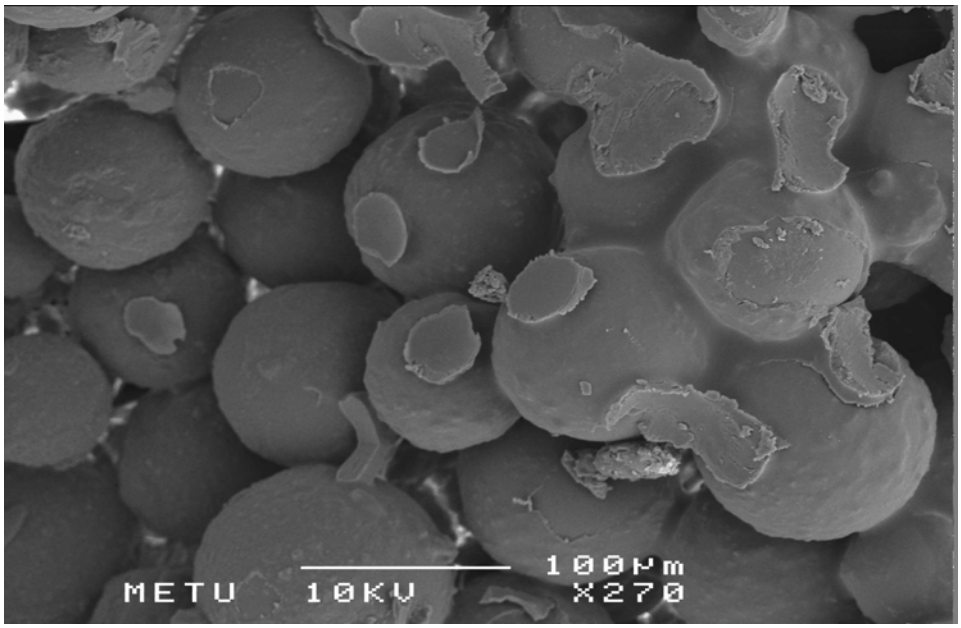

Figure 3.25. SEM photomicrograph of the sample prepared with poly(MMA-HEMA) copolymer microspheres having 5% HEMA content, VMD of 48µm, and epoxy solution with 10% epoxy content. (side, X270)

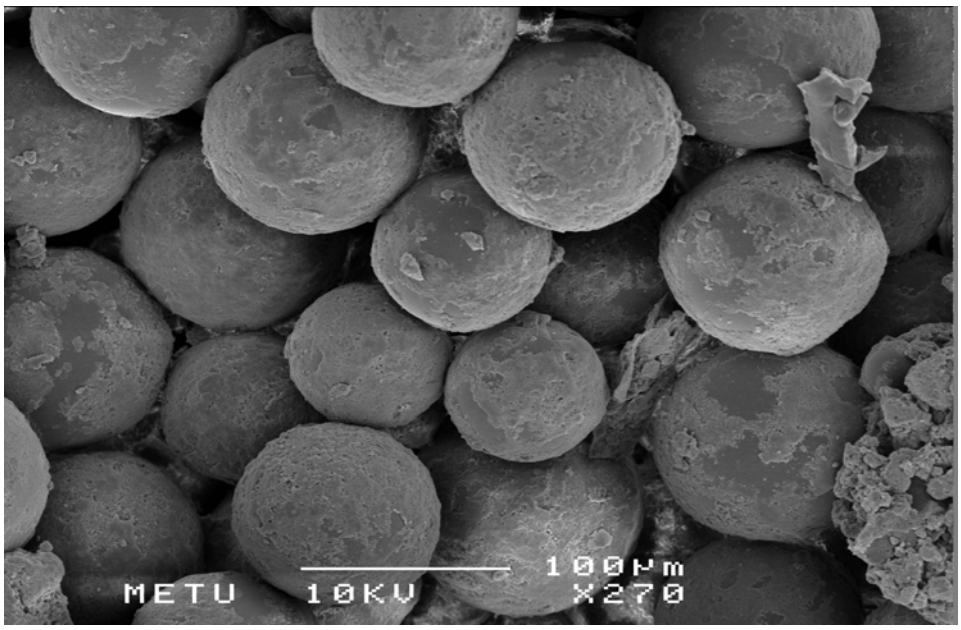

Figure 3.26. SEM photomicrograph of the sample prepared with poly(MMA-HEMA) copolymer microspheres having 5% HEMA content, VMD of 48µm, and epoxy solution with 10% epoxy content. (middle, X270)

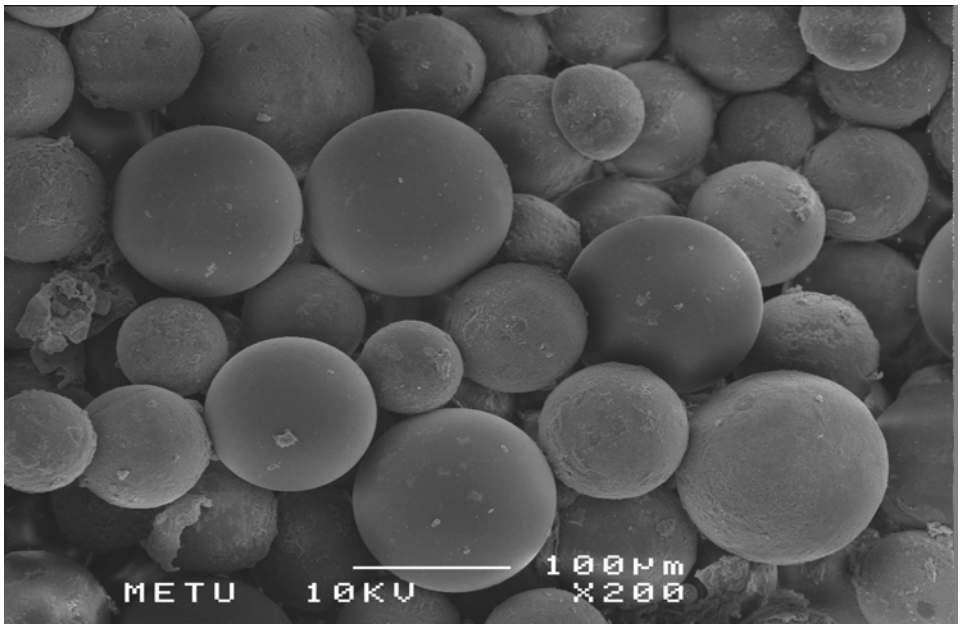

Figure 3.27. SEM photomicrograph of the sample prepared with poly(MMA-HEMA) copolymer microspheres having 15% HEMA content, VMD of 47µm, and epoxy solution with 5% epoxy content. (X200)

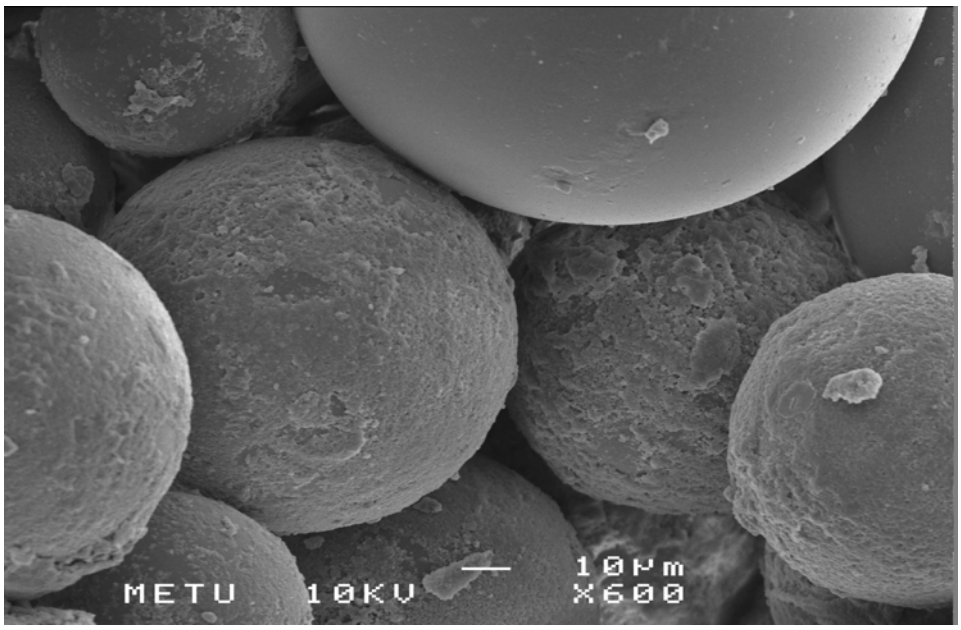

Figure 3.28. SEM photomicrograph of the sample prepared with poly(MMA-HEMA) copolymer microspheres having 15% HEMA content, VMD of 47µm, and epoxy solution with 5% epoxy content. (X600)

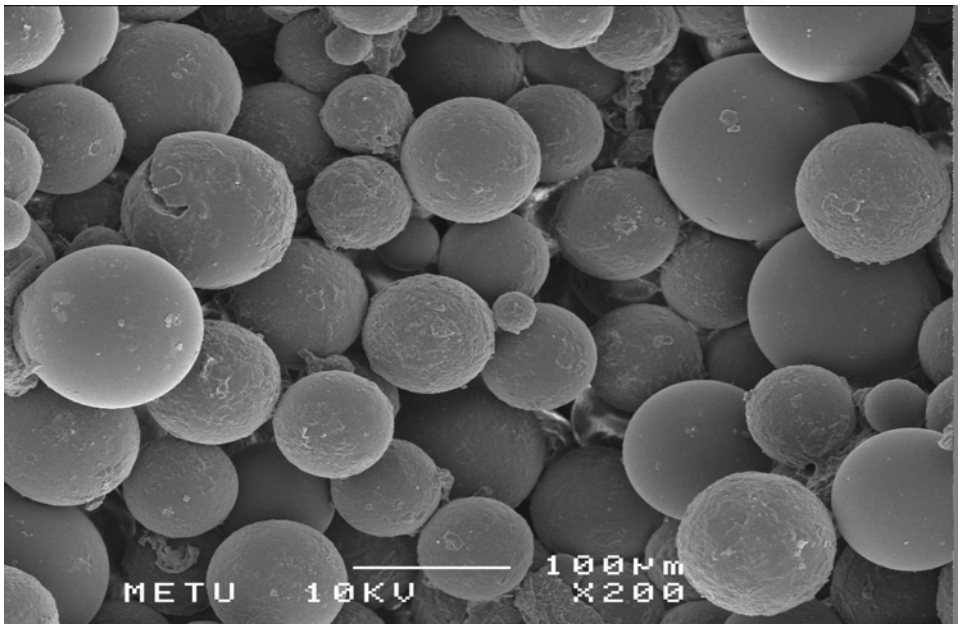

Figure 3.29. SEM photomicrograph of the sample prepared with poly(MMA-HEMA) copolymer microspheres having 15% HEMA content, VMD of 47µm, and epoxy solution with 10% epoxy content. (X200)

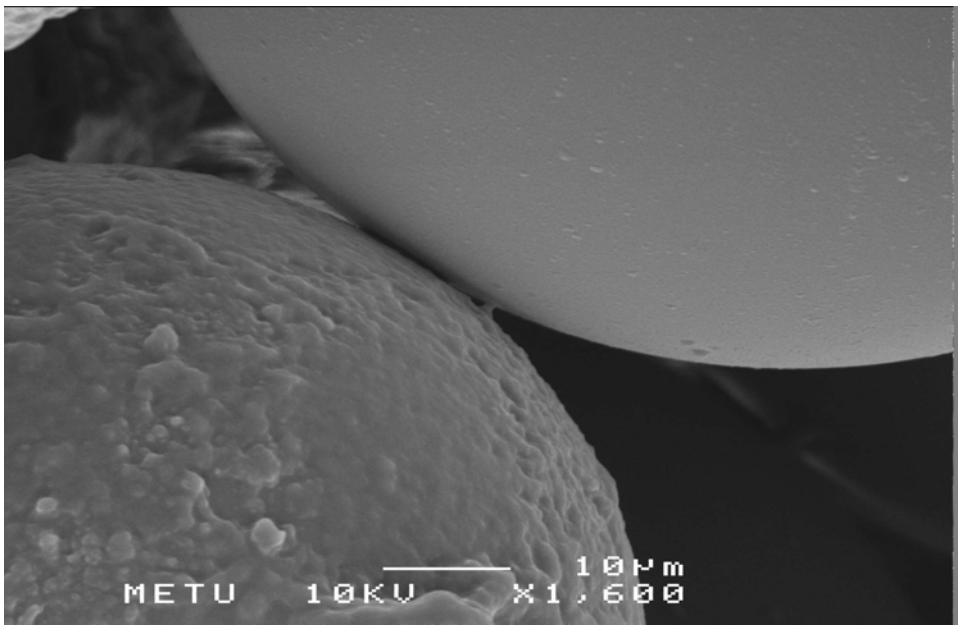

Figure 3.30. SEM photomicrograph of the sample prepared with poly(MMA-HEMA) copolymer microspheres having 15% HEMA content, VMD of 47µm, and epoxy solution with 10% epoxy content. (X1600)

3.8. Capillary Imregnation

In this study, the amount and rate of water impregnation into cylindrical porous samples were measured by the weight decrease of water due to its uptake. The data, collected in terms of weight change, was converted to height by the equation below. (It is assumed that water fills all the capillaries).

$$W = h \pi R^2 P \rho \qquad (15)$$

where W and h are the weight (g) and height (cm) of water impregnated, R and P are the radius(cm) and porosity (%) of cylindrical sample and ρ (g/cm^3) is the density of water. The measured time (s) versus height (m) data are given in Appendix. Figure 3.31 represents height (m) vs time (s) graph for the impregnation of water through the capillary-porous polymer samples for the first 20 seconds.

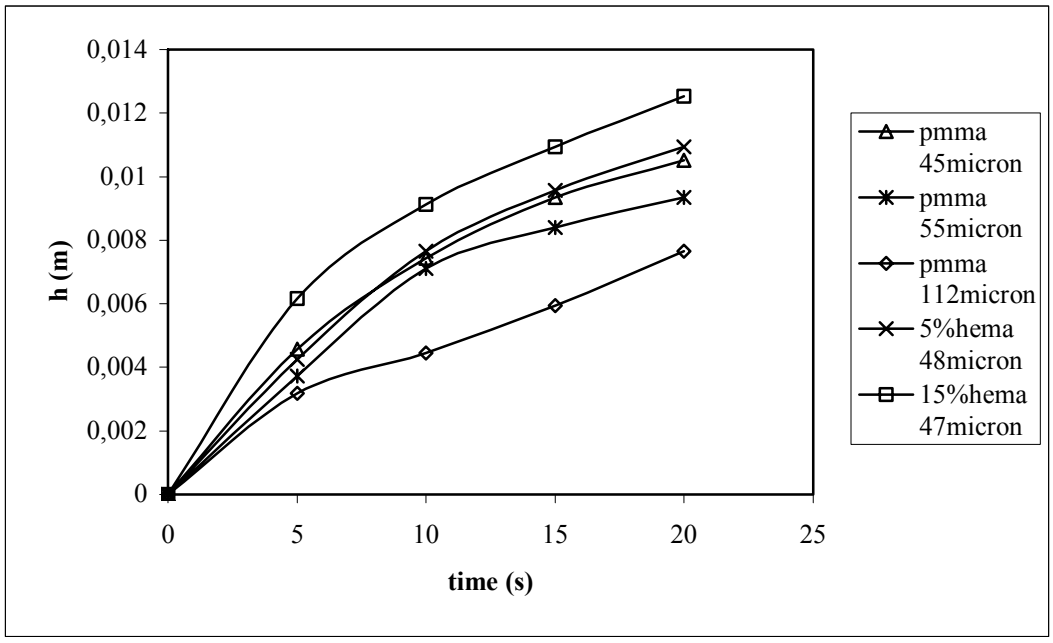

Figure 3.31. height (m) versus time (s) graph for the impregnation of water through the porous polymer samples for the first 20 seconds.

The rate of impregnation is higher for the samples prepared with poly(MMA-HEMA) copolymer beads than for the samples with PMMA microspheres. Comparing the results only for copolymers, it is observed that as the HEMA content increases rate of impregnation increases. As reported in Table 3.6 the contact angles of polymers with water decreases with the increasing HEMA content. Therefore, we expect that poly(MMA-HEMA) copolymer with 15% HEMA content must have better wettability and higher impregnation rate.

For the samples prepared with PMMA beads, as the VMD of microspheres increases, rate of impregnation decreases. The tendency can be explained by particle size distribution of the microspheres in the samples and the resultant capillary radii. As it is seen from the particle size distribution curves (Figures 3.6 to 3.10), PMMA microspheres polymerized at 400 rpm stirring rate, have the broadest particle size distribution and the largest mean particle diameter (112 μm). The abundance of smaller particles results in occupation of interstices, thus diminishing the overall voidage and representative capillary radii. Therefore, as the particle size distribution broadens, the rate of impregnation decreases.

For a capillary of constant cross-sectional geometry, it is assumed that at the initial instant t=0, a liquid just touches the bottom of the capillary with the height, h, being zero. Neglecting end effects and gravitational forces and assuming that the fluid is a Newtonian liquid with viscosity μ, a quasi-steady state creeping flow analysis gives the Lucas-Washburn equation [19];

$$h = A\, t^{1/2} \qquad (16)$$

where $A= (\gamma\, R_c\, \cos\theta\, /\, 2\mu)^{1/2}$ with R_c being a representative capillary radius, γ being the surface tension, and θ being the contact angle between the liquid and the capillary walls. The Lucas-Washburn equation holds for very small capillaries.

The initial slopes of the graphs (Figures 3.32-3.36) give us the constant A in the Lucas-Washburn equation. We have found $h \alpha t^{1/2}$ in all of the experiments at the early times. Due to finite size of the sample, the impregnation process deviates from linearity when large pores are filled towards the end of an experiment and water is filling the smallest pores only. Finding A, the representative capillary radii R_c of all the samples were calculated and presented in Table 3.10. For this calculation, the surface tension (γ) of water was taken as 0.0728 N/m [18], the viscosity (μ) of water as 0.01 poise and the contact angles (θ) between water and pure PMMA, 5% and 15% HEMA copolymers as 73.09, 71.82 and 69.44 respectively.

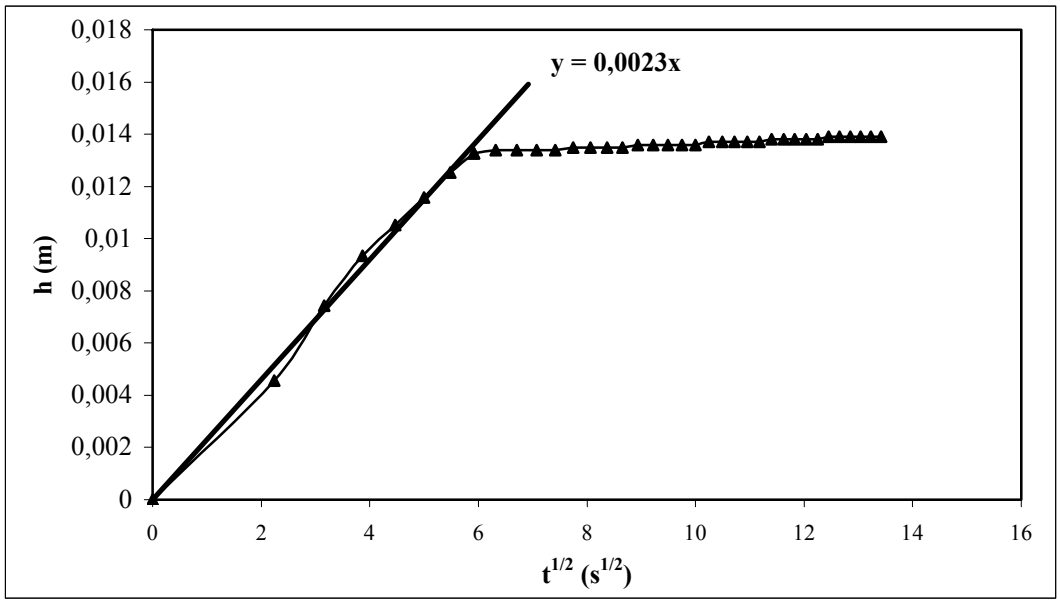

Figure 3.32. h (m) versus $t^{1/2}(s^{1/2})$ graph for the impregnation of water through cylindrical porous sample prepared with PMMA beads having VMD of 45μm.

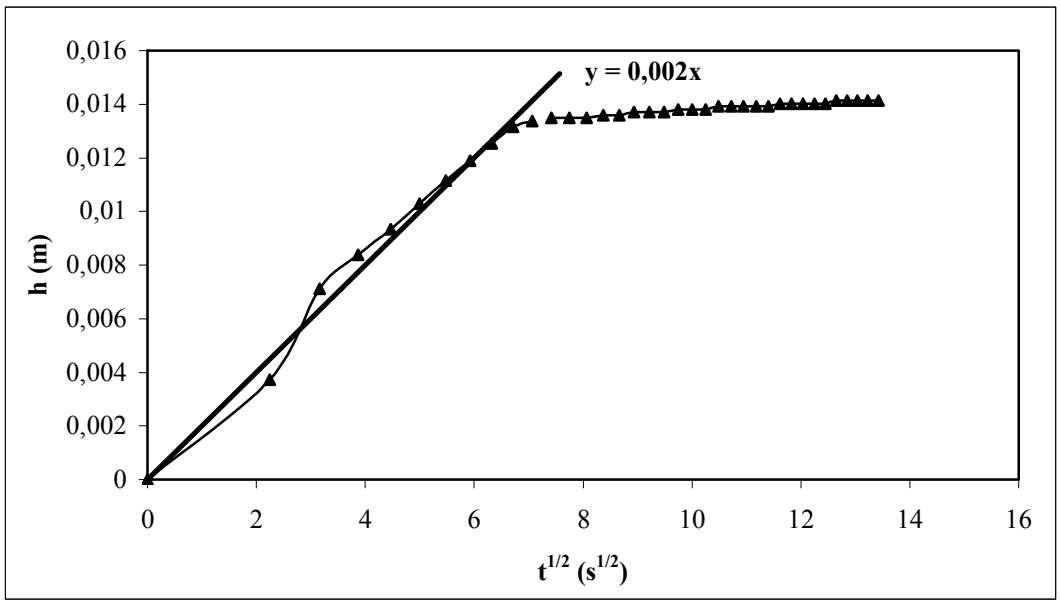

Figure 3.33. h (m) versus $t^{1/2}(s^{1/2})$ graph for the impregnation of water through cylindrical porous sample prepared with PMMA beads having VMD of 55 μm.

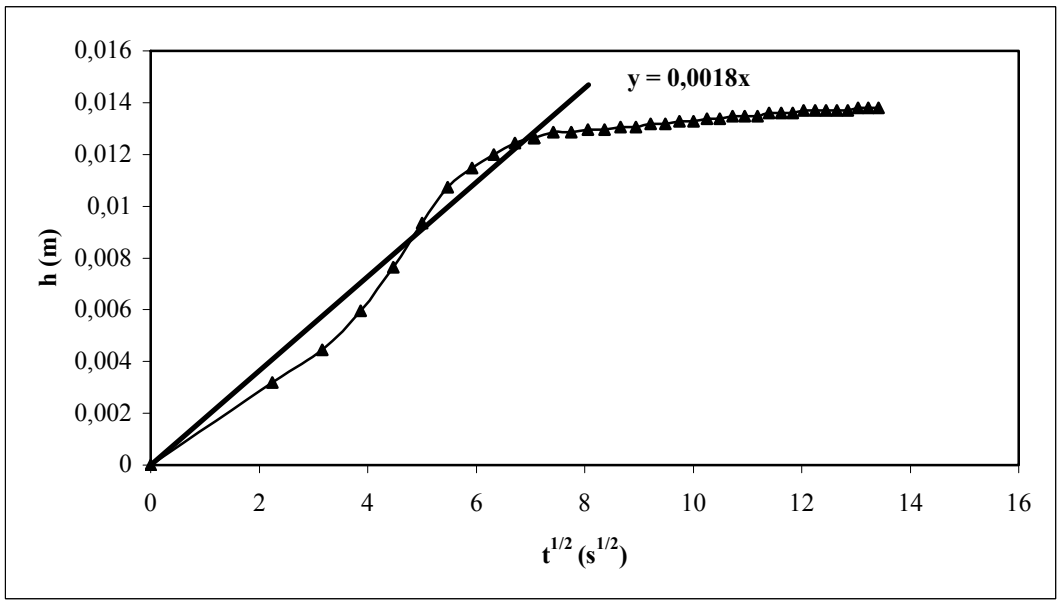

Figure 3.34. h (m) versus $t^{1/2}(s^{1/2})$ graph for the impregnation of water through cylindrical porous sample prepared with PMMA beads having VMD of 112 μm.

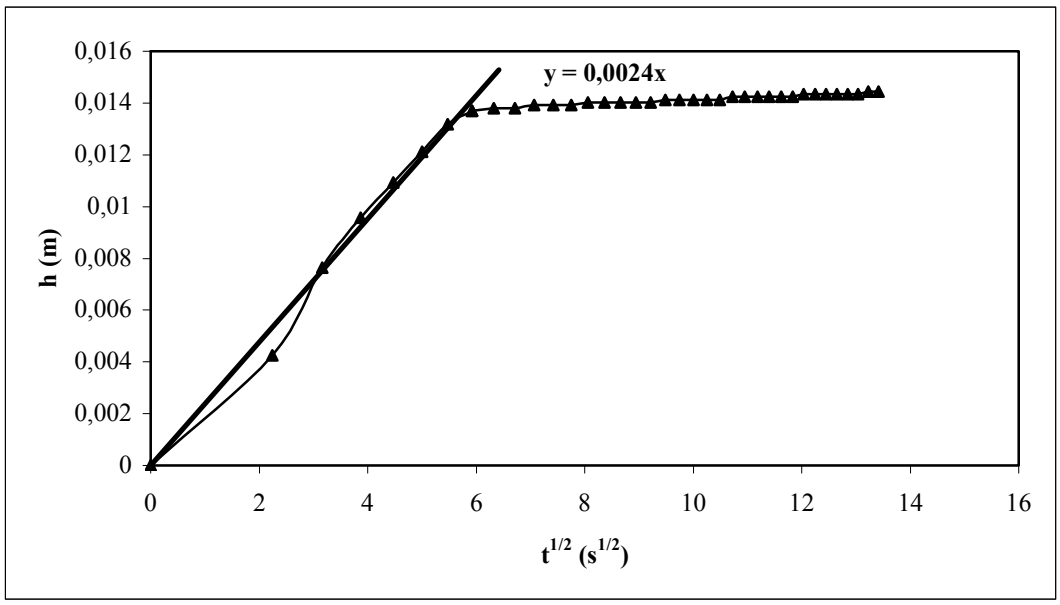

Figure 3.35. h (m) versus $t^{1/2}(s^{1/2})$ graph for the impregnation of water through cylindrical porous sample prepared with poly(MMA-HEMA) copolymer beads having 5% HEMA content and VMD of 48 μm.

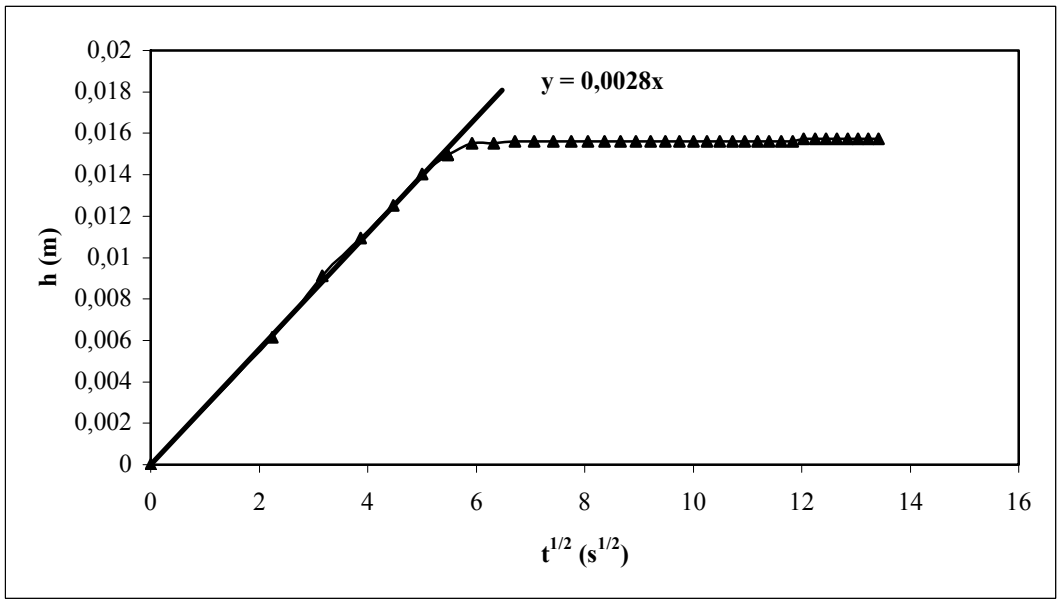

Figure 3.36. h (m) versus $t^{1/2}(s^{1/2})$ graph for the impregnation of water through cylindrical porous sample prepared with poly(MMA-HEMA) copolymer beads having 15% HEMA content and VMD of 47 μm.

Table 3.10. Calculated representative capillary radii of porous polymer samples

Composition and VMD of microspheres in the sample	**Representative capillary radius (μm) (R_c)**
PMMA, 45μm	5.01
PMMA, 55μm	3.79
PMMA, 112μm	3.07
Poly(MMA-HEMA) (5%HEMA),48μm	4.69
Poly(MMA-HEMA) (15%HEMA),47μm	5.72

Particle size analysis results (Table 3.3) are also in line with the calculated representative capillary radius values. The samples being composed of microspheres with VMD of 45-48 μm have a narrow particle size distribution with respect to others and therefore they must have larger capillary radii. Due to its broader particle size distribution, sample containing PMMA microspheres with VMD of 112 μm has a denser packing and therefore the smallest representative capillary radius.

CHAPTER 4

CONCLUSIONS

A novel method of creating a porous matrix by random packing of suspension polymerized acrylic spheres is achieved in this study. The porosity and the impregnation kinetics of the porous matrices are qualitatively related to the particle size and particle size distribution of the spherical particles. The idea of inter-connecting the spheres to each other by liquid bridge formation and the subsequent polymerization and the solidification of the liquid bridges is achieved experimentally. The bridge formation is carried out by an epoxy plus hardener solution and the evaporation of the solvent prior to the hardening of the epoxy system.

In theory water soluble acrylic polymers such as methacrylic acid or acrylic acid can also be used with cross-linking difunctional acrylic monomers instead of epoxy based system.

The required strengths of the porous matrices is better obtained when the binder solution used has 10% epoxy plus hardener content.

In terms of pore space creation less polydisperse spheres are feasible and in general pore volume, polydispersity, and the surface energy of the spheres can be utilized to prepare matrices with the required impregnation values.

The use of hydrophilic monomers in the copolymer structure is instrumental in reducing the contact angle value for better impregnation. The percentage of the water soluble acrylic can also be increased above the 15% value used in this study with the incorporation of cross-linking agent during the production of microspheres.

In theory the method is not restricted to micron size spheres and micron size capillaries which are investigated here. Even nanosize porosities can be prepared with the use of nano-particles employing a very similar technique used in this study.

It is believed that from a scientific and technological point of view a successful and robust method is developed for the production of porous substrates.

REFERENCES

[1] Siwy Z., Apel P., Dobrev D., Neumann R., Spohr R., Trautmann C., Voss K., *Ion Transport Through Asymmetric Nanopores Prepared by Ion Track Etching,* Nuclear Instruments and Methods in Physics Research, Vol. 208, 143-148, 2003.

[2] Kansal A.R., Torquato S., Stillinger F.H., *Computer Generation of Dense Polydisperse Sphere Packings,* Journal of Chemical Physics, Vol. 117, 8212-8218, 2002.

[3] Dullien F.A.L., *Porous Media: Fluid Transport and Pore Structure*, Academic Press Inc., New York, 1992.

[4] http://www.magicpump.com.tw/e_equ-b_m.htm

[5] Novak W.R., Lesko M.P, *Kirk-Othmer Encyclopedia of Chemical Technology*, 4th edition, 506-537, Wiley, New York, 1991.

[6] Glavis F.J., *Hydrolysis of Crystallizable Poly(methyl methacrylate)*, Journal of Polymer Science, Vol. 36, 547-549, 1959.

[7] Cholod M.S., Parker H., *Polymeric Materials Encyclopedia*, CRC Press Inc., 6385-6390, 1996.

[8] Hsieh K.H., Young T.H., *Polymeric Materials Encyclopedia*, CRC Press Inc., 3087-3091, 1996.

[9] Ho C.C., Khew M.C., *Surface Free Energy Analysis of Natural and Modified Natural Rubber Latex Films by Contact Angle Method*, Langmuir, Vol. 16, 1407-1414, 2000.

[10] Sipahi C., Anil N., Bayramli E., *The Effect of Acquired Salivary Pellicle on the Surface Free Energy and Wettability of Different Denture Base Materials*, Journal of Dentistry, Vol. 29, 197-204, 2001.

[11] Akovali G., Torun T.T., Bayramli E., Erinç N.K., *Mechanical Properties and Surface Energies of Low Density Polyethylene-poly(vinyl chloride) blends*, Polymer, Vol. 39, 1363-1368, 1998.

[12] Van Oss C.J., Chaudhury M.K., Good R.J., *Additive and Non-additive Surface Tension Components and the Interpretation of Contact Angles*, Langmuir, Vol. 4, 884-891, 1988.

[13] Bezrukov A., Stoyan D., Bargiel M., *Spatial Statistics for Simulated Packings of Spheres*, Image Analysis and Stereology, Vol. 20, 203-206, 2001.

[14] Ouchiyama N., Tanaka T., *Porosity Estimation from Particle Size Distribution*, Industrial and Engineering Chemistry Fundamentals, Vol. 25, 125-129, 1986.

[15] Sohn H.Y., Moreland C., *The Effect of Particle Size Distribution on Packing Density*, The Canadian Journal of Chemical Engineering, Vol. 46, 162-167, 1968.

[16] Gray W.A., *The Packing of Solid Particles*, Chapman and Hall, London, 1968.

[17] Bayramli E., van de Ven, *An Experimental Study of Liquid Bridges between Spheres in a Gravitational Field,* Journal of Colloid and Interface Science, Vol. 116 (2), 503- 510, 1987.

[18] Kornev K.G., Neimark A.V., *Spontaneous Penetration of Liquids into Capillaries and Porous Membranes Revisited*, Journal of Colloid and Interface Science, Vol. 235, 101-113, 2001.

[19] Bayramli E., Powell R.L., *Impregnation Dynamics of Carbon Fiber Tows*, Journal of Composite Materials, Vol. 26, 1427-1442, 1992.

APPENDIX

Table A.1. t (s) versus amount of water (g) and corresponding h (m) data for the impregnation of water through cylindrical porous sample prepared with PMMA beads having VMD of 45 μm.

t (s)	water (g)	h (m)	t (s)	water (g)	h (m)
0	0	0	95	1.28	0.013595
5	0.43	0.004567	100	1.28	0.013595
10	0.70	0.007435	105	1.29	0.013701
15	0.88	0.009346	110	1.29	0.013701
20	0.99	0.010515	115	1.29	0.013701
25	1.09	0.011577	120	1.29	0.013701
30	1.18	0.012533	125	1.29	0.013701
35	1.25	0.013276	130	1.30	0.013807
40	1.26	0.013382	135	1.30	0.013807
45	1.26	0.013382	140	1.30	0.013807
50	1.26	0.013382	145	1.30	0.013807
55	1.26	0.013382	150	1.30	0.013807
60	1.27	0.013489	155	1.31	0.013913
65	1.27	0.013489	160	1.31	0.013913
70	1.27	0.013489	165	1.31	0.013913
75	1.27	0.013489	170	1.31	0.013913
80	1.28	0.013595	175	1.31	0.013913
85	1.28	0.013595	180	1.31	0.013913
90	1.28	0.013595			

Table A.2. t (s) versus amount of water (g) and corresponding h (m) data for the impregnation of water through cylindrical porous sample prepared with PMMA beads having VMD of 55 μm.

t (s)	water (g)	h (m)	t (s)	water (g)	h (m)
0	0	0	95	1.30	0.013807
5	0.35	0.003717	100	1.30	0.013807
10	0.67	0.007116	105	1.30	0.013807
15	0.79	0.008390	110	1.31	0.013913
20	0.88	0.009346	115	1.31	0.013913
25	0.97	0.010300	120	1.31	0.013913
30	1.05	0.011152	125	1.31	0.013913
35	1.12	0.011895	130	1.31	0.013913
40	1.18	0.012533	135	1.32	0.014020
45	1.24	0.013170	140	1.32	0.014020
50	1.26	0.013382	145	1.32	0.014020
55	1.27	0.013489	150	1.32	0.014020
60	1.27	0.013489	155	1.32	0.014020
65	1.27	0.013489	160	1.33	0.014126
70	1.28	0.013595	165	1.33	0.014126
75	1.28	0.013595	170	1.33	0.014126
80	1.29	0.013701	175	1.33	0.014126
85	1.29	0.013701	180	1.33	0.014126
90	1.29	0.013701			

Table A.3. t (s) versus amount of water (g) and corresponding h (m) data for the impregnation of water through cylindrical porous sample prepared with PMMA beads having VMD of 112 μm.

t (s)	water (g)	h (m)	t (s)	water (g)	h (m)
0	0	0	95	1.25	0.013276
5	0.30	0.003186	100	1.25	0.013276
10	0.42	0.004461	105	1.26	0.013382
15	0.56	0.005948	110	1.26	0.013382
20	0.72	0.007647	115	1.27	0.013489
25	0.88	0.009346	120	1.27	0.013489
30	1.01	0.010727	125	1.27	0.013489
35	1.08	0.011471	130	1.28	0.013595
40	1.13	0.012002	135	1.28	0.013595
45	1.17	0.012427	140	1.28	0.013595
50	1.19	0.012639	145	1.29	0.013701
55	1.21	0.012851	150	1.29	0.013701
60	1.21	0.012851	155	1.29	0.013701
65	1.22	0.012958	160	1.29	0.013701
70	1.22	0.012958	165	1.29	0.013701
75	1.23	0.013064	170	1.30	0.013807
80	1.23	0.013064	175	1.30	0.013807
85	1.24	0.013170	180	1.30	0.013807
90	1.24	0.013170			

Table A.4. t (s) versus amount of water (g) and corresponding h (m) data for the impregnation of water through cylindrical porous sample prepared with poly(MMA-HEMA) copolymer beads having 5% HEMA content and VMD of 48 μm.

t (s)	water (g)	h (m)	t (s)	water (g)	h (m)
0	0	0	95	1.33	0.014126
5	0.40	0.004248	100	1.33	0.014126
10	0.72	0.007647	105	1.33	0.014126
15	0.90	0.009559	110	1.33	0.014126
20	1.03	0.010940	115	1.34	0.014232
25	1.14	0.012108	120	1.34	0.014232
30	1.24	0.013170	125	1.34	0.014232
35	1.29	0.013701	130	1.34	0.014232
40	1.30	0.013807	135	1.34	0.014232
45	1.30	0.013807	140	1.34	0.014232
50	1.31	0.013913	145	1.35	0.014338
55	1.31	0.013913	150	1.35	0.014338
60	1.31	0.013913	155	1.35	0.014338
65	1.32	0.014020	160	1.35	0.014338
70	1.32	0.014020	165	1.35	0.014338
75	1.32	0.014020	170	1.35	0.014338
80	1.32	0.014020	175	1.36	0.014444
85	1.32	0.014020	180	1.36	0.014444
90	1.33	0.014126			

Table A.5. t (s) versus amount of water (g) and corresponding h (m) data for the impregnation of water through cylindrical porous sample prepared with poly(MMA-HEMA) copolymer beads having 15% HEMA content and VMD of 47 μm.

t (s)	water (g)	h (m)	t (s)	water (g)	h (m)
0	0	0	95	1.47	0.015613
5	0.58	0.006160	100	1.47	0.015613
10	0.86	0.009134	105	1.47	0.015613
15	1.03	0.010939	110	1.47	0.015613
20	1.18	0.012533	115	1.47	0.015613
25	1.32	0.014020	120	1.47	0.015613
30	1.41	0.014976	125	1.47	0.015613
35	1.46	0.015507	130	1.47	0.015613
40	1.46	0.015507	135	1.47	0.015613
45	1.47	0.015613	140	1.47	0.015613
50	1.47	0.015613	145	1.48	0.015719
55	1.47	0.015613	150	1.48	0.015719
60	1.47	0.015613	155	1.48	0.015719
65	1.47	0.015613	160	1.48	0.015719
70	1.47	0.015613	165	1.48	0.015719
75	1.47	0.015613	170	1.48	0.015719
80	1.47	0.015613	175	1.48	0.015719
85	1.47	0.015613	180	1.48	0.015719
90	1.47	0.015613			